UNIVERSITÉ 8 Mai 1945 - Guelma
Faculté des Sciences et de la Technologie
Département de Génie Mécanique

Mémoire de Fin d'Etudes

Présenté par: **Bordjiba Nidhal**

Master 2

Option: Construction Mécanique

==========

Design and CFD Analysis of Diverse Convergent-Divergent Nozzle Profiles

==========

Sous la Direction de
Pr. A. HADDAD
L. DAI

Année universitaire 2023/2024

ملخص
ABSTRACT
Résumé

في مجال الديناميكا الهوائية، تلعب التدفقات الأسرع من الصوت دورًا مهمًا نظرًا لخصائصها الفريدة وتطبيقاتها المبتكرة. يتناول هذا العمل تصميم وتحليل الفوهات الأسرع من الصوت من نوع "دي-لافال" عن طريق تطبيق طريقة الخصائص (MoC) ومحاكاة CFD باستخدام برنامج "ANSYS-Fluent". كما تم تصميم ومحاكاة ثلاثة وألغ من الأشكال: الشكل الكلاسيكي المخروطي، الشكل الأكثر تقدما ً المعروف باسم الملف الدائري أو "الكنتوري"، وأخيرًا الشكل الأكثر جرأة والذيعرف عمومًا بالمفتوح. تم محاكاة الأشكال المختلفة المتباينة باستخدام خط مستقيم، متعددة الحدود من الدرجة الثانية، ودالة أسية. القسم "المتقارب" (convergent) هو نفسه لجميع لأشكال حيث أنة يوصل فقط إلى سرعات دون صوتية عند االخنق (col). أظهرت النتائج التي تم الحصول عليها تفوق الشكل الدائري "الكنتوري" على الفوهات الأخرى.

In the field of aerodynamics, supersonic flows play a significant role due to their unique properties and innovative applications. This work focuses on the design and analysis of de-Laval type supersonic nozzles using the Method of Characteristics (MoC) and CFD simulation with ANSYS-Fluent. Three types of profiles are designed and simulated: the classic conical contour, the more advanced contour known as the bell-shaped profile, and finally a more daring contour generally referred to as open. The profiles of the different divergent sections are simulated by a straight line, a second-degree polynomial, and an exponential function respectively. The convergent section is the same for all profiles as it serves only to expand the flow to reach subsonic speeds at the throat. The results obtained show the superiority of the bell-shaped profile over the other two nozzles.

Dans le domaine de l'aérodynamique, les écoulements supersoniques jouent un rôle important en raison de leurs propriétés uniques et de leurs applications innovantes. Le présent travail s’intéresse à la conception et l'analyse de tuyères supersoniques de type de-Laval par application de la Méthode des Caractéristiques (MoC) et la simulation CFD par ANSYS-Fluent. Trois types de profils sont conçus et simulés: le contour classique conique, celui plus avancé connu sous le nom de profil contour ou en cloche, et enfin un contour plus audacieux généralement dénommé ouvert. Les profils des différentes sections divergentes sont simulés par une droite, un polynôme du second degré et une fonction exponentielle respectivement. La section convergente est la même pour tous les profils car servant uniquement à détendre l’écoulement pour lui faire atteindre des vitesses subsoniques au col. Les résultats obtenus montrent une prépondérance du profil contour sur les deux autres tuyères.

ACKNOWLEDGMENTS

First and foremost, I would like to thank Allah for granting me the strength, courage, and determination to complete this modest work.

I would like express my heartfelt gratitude to my supervisor, **Prof. A. Haddad**, for his assistance, guidance, and availability throughout the development of this dissertation.

I also extend my thanks to **Doct. L. Dai** for her availability and contribution especially during the application of numerical simulations.

My gratitude also goes to the members of the jury for agreeing to evaluate this work, and not forgetting all the faculty members of the Mechanical Engineering Department of 8th May 1945-Guelma university.

Lastly, my sincere thanks to all who have contributed directly or indirectly to the completion of this work.

LIST OF CONTENTS

LIST OF FIGURES

LIST OF TABLES

NOTATION

Coordinate system

x	[m]	Axial coordinate direction,
y	[m]	Radial coordinate direction,
u	[m/s]	Axial component of the velocity,
v	[m/s]	Radial component of the velocity.

Latin notation:

a	[m/s]	Speed of sound
A	[m^2]	Area or Attachment point
A_w, B_w, C_w	[-]	2^{nd}-order polynomial wall coefficients
C_p	[m^2/s^2]	Specific heat at constant pressure
C_T	[-]	Thrust coefficient
D_ω	[m^2/s^3]	Cross-diffusion term in the transport equations (SST k-ω model)
g	[m/s^2]	representative variable or gravity acceleration
$\tilde{G}_k$	[$kg/m.s^3$]	Generation of k due to mean velocity gradients (SST k-ω model)
G_ω	[$kg/m^3.s$]	Generation of ω due to mean velocity gradients (SST k-ω model)
I_{sp}	[s]	Specific impulse
k	[m^2/s^2]	Turbulent kinetic energy or conductibility coefficient
$\dot{m}$	[kg/s]	Mass flow rate
M	[-]	Mach number
n	[-]	number of moles of the gas
P	[N/m^2]	Pressure
P_a	[N/m^2]	Ambient pressure or Pascal
P_t	[N/m^2]	Total (or stagnation) pressure
R	[J/mol.K]	Universal gas constant
R_G	[$kg.m^2/s^2$]	Specific gas constant
R_{td}	[m]	Downstream throat radius of curvature
R_{tu}	[m]	Upstream throat radius of curvature
T	[K]	Temperature
T_t	[K]	Total (or stagnation) temperature
V	[m/s]	Velocity
ϑ	[m^3]	Volume
x_A, y_A	[m]	Attachment point axial and radial coordinates
x_e	[m]	Nozzle length
Y_k	[m^2/s^3]	Dissipation of k due to turbulence (sst k-ω model)
Y_ω	[1/s]	Dissipation of ω due to turbulence (sst k-ω model)
y_E	[m]	Nozzle radius at exit
y_t	[m]	Throat radius

Greek notation:

A	[-]	Angle
γ	[-]	Specific heat ratio ($\gamma=C_p/C_v$)
θ	[-]	Angle
θ_A	[-]	Attachment angle
θ_e	[-]	Exit angle
λ	[-]	Correction factor in conical nozzles
μ	[kg/m.s]	Dynamic viscosity
ν	[m^2/s]	Kinematic viscosity
ρ	[kg/m^3]	Density
σ	[kg/m.s^2]	Normal stress
σ_{ij}	[kg/m.s^2]	Stress tensor
σ_k	[-]	Turbulent Prandtl number for k
σ_ω	[-]	Turbulent Prandtl number for ω
τ	[kg/m.s^2]	Shear stress
ω	[1/s]	Specific turbulent dissipation rate

Subscripts and superscripts:

$(\ )_a$	Ambient state
$(\ )_e$	Exit state
$(\ )_{eff}$	Effective state
$(\ )_t$	Total (or stagnation) state
$(\ )_w$	Wall state
$\bar{(\ )}$	Average value of property
$(\ )'$	Fluctuation of property

Acronyms:

2-D	Two-Dimensional
C-D	Convergent-Divergent
CFD	Computational Fluid Dynamics
FDM	Finite-Difference Method
FVM	Finite Volume Method
MoC	Method of Characteristics
RANS	Reynolds-Averaged Navier-Stokes
SST	Shear Stress Transport

INTRODUCTION

Understanding the characteristics of axisymmetric supersonic nozzles is crucial for optimizing the performance of propulsion systems. By grasping the subtleties of flow behavior, nozzle design can be refined to maximize efficiency and enhance the performance of aerospace vehicles. Moreover, supersonic flows offer particular advantages for experimental and computational visualization, providing an interesting avenue for research while retaining essential flow characteristics.

In addition, studying supersonic flow fields gives designers greater flexibility in nozzle geometry, facilitating the development and adaptation of various configurations for specific applications. This knowledge is also crucial for thrust vectoring, a critical aspect of maneuverability and control in modern aerospace vehicles. However, these efforts also highlight persistent gaps in understanding and implementing design processes, particularly concerning performance optimization and integrating different nozzle geometries.

This work applies a design methodology using Fortran language represented by the Method of Characteristics, incorporates simulations using 'ANSYS-Fluent' in order to compare various nozzle geometries. It aims to fill this gap by proposing a simple, efficient, and practical approach for the design and optimization of supersonic nozzles. By integrating these elements, this work offers a solution that could enhance current understanding while providing practical tools.

In this context, the present thesis is divided into four chapters. The first chapter lays the theoretical foundations by exploring the fundamental characteristics of supersonic flows and examining the modeling and analysis methods used.

The second chapter focuses on applying the Method of Characteristics to design three different nozzle profiles: a conical approached by a straight line, a contoured or bell-shaped approached by a 2^{nd}-oder polynomial and finally an open geometry approached by an exponential. The analysis has been concentrating on the divergent supersonic sections.

The third chapter details the methodology used to analyze these profiles using CFD simulations with 'ANSYS-Fluent,' covering model preparation, mesh generation, computations, and results gathering in terms of performances.

Finally, the fourth chapter presents the results obtained and compares the performance of the various profiles represented by the conical, contour, and open geometries in order to try and identify the optimal profile that might be used for the propulsion of various propulsion engines.

Chapitre1:

LITERATURE REVIEW

1.1 GENERAL

In the field of modern aerodynamics, supersonic flows represent a crucial area of study due mainly to their unique properties and innovative applications. This first chapter delves deeply into these flows, highlighting their fundamental characteristics and dynamic behavior. The present chapter particularly focuses on C-D type supersonic nozzles, as well as advanced numerical methods such as the method of characteristics and the finite volume method, implemented through FLUENT software, to model and analyze these complex phenomena.

1.2 THE COMPRESSIBLE FLOW

1.2.1 Definition and Importance of Compressible Flow

Compressible fluid refers to a type of fluid that can change its volume significantly in response to changes in pressure or temperature. The compressibility of fluids, a measure of how density changes with pressure, distinguishes gases as highly compressible and most liquids as nearly incompressible. In fluid dynamics, pressure variations, often tied to velocity changes, induce density shifts, impacting the flow. The influence of compressibility is evident in aerodynamic design with aircrafts featuring distinct design adaptations to counter compressibility effects. While originally crucial for high-speed aircraft design, compressible fluid flow theory finds broad applicability across fields where density and temperature changes significantly affect flow dynamics [1].

1.2.2 Brief historical development

The study of compressible flows has a rich history that dates back to the early 19th century, initially spurred by investigations into the behavior of fired bullets, which led to advancements in gun accuracy and artillery capabilities. That era marked the inception of gas dynamics research. Gustaf de Laval's contributions, including the development of the de Laval nozzle that enabled gas acceleration to supersonic speeds, further propelled the field forward. Ernst Mach's experiments added crucial insights into the physical phenomena underlying gas dynamics.

In the early 20th century, attention shifted towards aerospace endeavors, with Ludwig Prandtl and his students introducing groundbreaking concepts such as boundary layers, supersonic shock waves, and nozzle design at the University of Göttingen, Germany. Prandtl's work laid the groundwork for modern aerodynamics. Theodore von Kármán, a student of Prandtl, continued to advance the understanding of supersonic flow alongside figures like

Meyer, Luigi Crocco, and Ascher Shapiro, who made significant contributions to gas dynamics principles.

In post-World War II, the emergence of jet engines and high-speed aircrafts prompted a deeper exploration of compressible flow. The term "sound barrier" encapsulated the technological hurdles encountered when nearing the speed of sound, necessitating breakthroughs for supersonic flight advancement. In the modern era, the study of compressible flows spans diverse applications, encompassing the design of high-speed aircraft, rocket motors, and understanding phenomena such as high-speed entry into planetary atmospheres and gas pipeline behavior [2-3-4].

1.2.3 Principal parameters of compressible flows

The various parameters and their interrelationships are the key to understanding and predicting the behavior of compressible flows in various applications, from aerospace engineering to weather forecasting.

1.2.3.1 The pressure

Pressure is one of the main properties of a fluid. It is defined as the ratio of the force to the surface area on which it is exerted, and is expressed in (Pa) or (N/m^2).

$$P = \frac{F}{S} \tag{1.1}$$

Pressure variations are prominent in compressible flows and are linked to changes in velocity and density through the Bernoulli equation for compressible flow.

1.2.3.2 The temperature

Temperature changes in a compressible flow are related to pressure changes through the ideal gas law and the concept of adiabatic processes. According to the ideal gas law ($Pv=nRT$), any change in pressure within a compressible flow will affect its temperature, assuming the volume remains constant. For an adiabatic process, the relationship between pressure (P), volume (v), and temperature (T) is described by the adiabatic relationship:

$$PV^{\gamma} = \text{constant} \tag{1.2}$$

where (γ) represents the specific heat ratio or adiabatic index.

1.2.3.3 The density

Density, noted (ρ), is the mass per unit volume of a fluid. It is measured in (kg/m³) in the SI system and slug/ft³ in the English system.1 Slug/ft³ = 515.363 kg/m³.

$$\rho = \frac{m}{v} \tag{1.3}$$

In compressible flows, density can change significantly with pressure and temperature. The variation of density is described by the equation of state for the fluid, typically the ideal gas law for perfect gases.

$$P\vartheta = nRT \tag{1.4}$$

1.2.3.4 The Mach number, (M)

Defined as the ratio of the flow velocity (c) to the speed of sound (a) The Mach number is a dimensionless quantity that is crucial in the study of compressible flows. It is defined as:

$$M = \frac{c}{a} \tag{1.5}$$

The Mach number determines the regime of the flow whether it is:

- Subsonic (M<1): In this case, the flow velocity is less than the speed of sound, and compressibility effects are usually negligible.
- Transonic (M≈1): The flow velocity is approximately equal to that of the sound. This regime is characterized by mixed flow regions where both subsonic and supersonic flows coexist, often resulting in significant compressibility effects.
- Supersonic (1<M<5): The flow velocity exceeds the speed of sound but is less than five times of it. This regime may involve shock waves and significant compressibility effects.
- Hypersonic (M>5): The flow velocity is greater than five times the speed of sound. This regime is characterized by extreme temperatures and pressures, with significant effects due to shock waves and high-temperature gas dynamics.

1.3 THE UNIVERSAL EQUATIONS DESCRIBING A COMPRESSIBLE FLOW

1.3.1 Continuity or conservation of mass equation

The conservation of mass principle states that mass cannot be created or destroyed. It states that within a control volume, the rate of mass entering the volume must equal that leaving it, under the assumption of steady flow and incompressible fluid. Its relation for a closed system undergoing a change may be expressed as:

$$m_{sys} = constant \Longrightarrow \frac{dm_{sys}}{dt} = 0 \tag{1.6}$$

In its differential form and for an unsteady flow, it comes:

$$\frac{\partial \rho}{\partial t} + \nabla \cdot (\rho V) = 0 \tag{1.7}$$

1.3.2 Navier-Stokes or conservation of momentum equation

The three fundamental laws of motion of Isaac Newton were stated in his work '*Philosophiæ Naturalis Principia Mathematica*' [5-6]. The conservation of momentum is a fundamental principle in physics, alongside the conservation of mass and the conservation of energy. It asserts that within a specific domain, the total momentum remains constant, and that it can only be altered by the action of forces. Defined as the product of an object's mass and its velocity, momentum is a vector quantity, possessing both magnitude and direction. Understanding momentum conservation is crucial for analyzing fluid flow problems, where properties may change in different directions.

The momentum equation may be expressed as:

$$\frac{\partial(\rho V)}{\partial t} + \nabla \cdot (\rho VV) = -\nabla p + \nabla \cdot \tau + \rho g \quad (1.8)$$

where (V) represents the velocity vector, (ρ) the density of the fluid, (p) the pressure, (τ) the viscous stress tensor, , (g) the external forces such as the gravitational forces, (∇) the divergence operator, and (VV) the dyadic product of the velocity vector with itself.

In their differential form, the Navier-Stokes equations named after mathematicians C.L. Navier and G. G. Stokes may expressed in their final form in cartesian coordinates as:

$$\begin{cases} \frac{\partial \rho}{\partial t} + \frac{\partial(\rho u_i)}{\partial x_i} = 0 \\ \rho\left(\frac{\partial u_i}{\partial t} + u_j \frac{\partial u_i}{\partial x_j}\right) = -\frac{\partial p}{\partial x_i} + \frac{\partial \tau_{ij}}{\partial x_j} + \rho g_i \end{cases} \quad (1.9)$$

The Navier-Stokes equations are derived assuming Newtonian fluid behavior, the density (ρ) can vary with pressure and temperature, the pressure (p) is a function of the state variables of the fluid, and cartesian coordinates (x_i) used to express spatial derivatives.

1.3.3 Conservation of energy equation

The first law of thermodynamics, also known as the conservation of energy principle provides the foundation for understanding the relationships between different forms of energy and their interactions. This principle states that energy can only change forms. The change in a system's energy content equals the difference between energy input and output, and this can be expressed as:

$$Ein - Eout = \Delta E \quad (1.10)$$

The energy content of a fixed quantity of mass (i.e. within a closed system) can be altered through two main mechanisms: heat transfer (Q) and work transfer (W). The conservation of energy for a fixed quantity of mass can be expressed in its rate form as:

$$\dot{Q}_{\text{net}} + \dot{w}_{\text{net}} = \frac{dE_{\text{sys}}}{dt} = \frac{d}{dt}\int_{\text{sys}} \rho e \, dv \quad (1.11)$$

This is the general expression of energy conservation for a fixed quantity of mass. For simple compressible systems, the total energy of the system consists of internal energy (U), kinetic energy (KE), and potential energy (PE). On a unit-mass basis, the total energy (e) is given by:

$$e = u + V^2/2 + gz \quad (1.12)$$

where:
- (u) is the internal energy per unit mass,
- $(V^2/2)$ is the kinetic energy per unit mass, with vv being the velocity,
- (gz) is the potential energy per unit mass.

1.3.4 Equation of state

One commonly used equation of state for gas flows assumes the gas behaves as an ideal gas, where intermolecular forces are negligible. This equation is:

$$p = \rho RT \quad (1.13)$$

1.4 CLOSURE OF THE SYSTEM OF EQUATIONS: THE TURBULENCE

1.4.1 The turbulent flow

Turbulence is a complex phenomenon in fluid dynamics characterized by chaotic changes in pressure and flow velocity. It occurs when the kinetic energy in parts of a fluid flow overcomes the damping effect of the fluid's viscosity, causing unsteady vortices of various sizes to interact with each other. The Reynolds number helps in understanding the balance between inertial and viscous forces in a fluid flow, which is crucial for analyzing the behavior of the flow, especially whether it is laminar or turbulent [7]. In 1883, Osborne Reynolds demonstrated this transition by regularly injecting dye into the midline of a pipe (Figure 1.1). In laminar flow, the dye forms a straight line and does not mix with the surrounding fluid: this is called the laminar flow. However, above a certain velocity, the sequence becomes unstable and the dye rapidly disperses throughout the entire pipe: this is the turbulent regime [8-9].

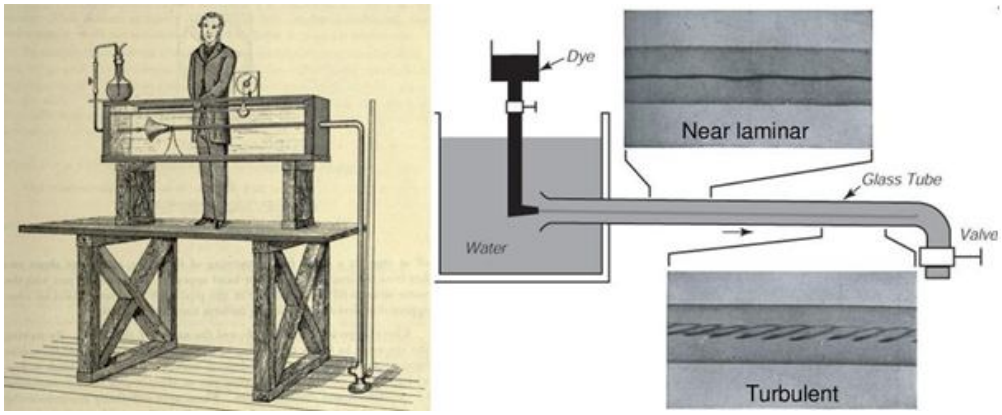

Figure 1.1 Experimental setup of the Reynolds experiment

The Reynolds number (Re) is a dimensionless quantity used in fluid mechanics to predict the flow regime in different fluid flow situations. It has been derived as the ratio of the inertial forces to the viscosity forces within a fluid and is given by the following expression:

$$Re = \frac{\rho V L}{\mu} = \frac{V L}{\nu} \tag{1.14}$$

where:
- (ρ) is the fluid density,
- (V) is the characteristic velocity,
- (L) is the characteristic length,
- (μ) is the dynamic viscosity of the fluid,
- (ν) is the kinematic viscosity of the fluid $\left(\nu = \frac{\mu}{\rho}\right)$.

1.4.2 Reynolds-Averaged Navier-Stokes (RANS) equations

The computations of the flow expansion within a nozzle have been performed through the application of the Reynolds-Averaged Navier-Stokes (RANS) equations in 2-D. These equations are favored due to their quicker computational turnaround time and the possibility of incorporation of suitable turbulence models for closure.

The governing equations comprise the continuity equation that has been stated earlier, but may be expressed as:

$$\frac{\partial}{\partial x}(\rho u_i) \tag{1.15}$$

The RANS and the energy equations are given by [10]:

$$\frac{\partial}{\partial xi}(\rho u_i u_j) = -\frac{\partial p}{\partial x_i} + \frac{\partial}{\partial x_j}\left[\mu\left(\frac{\partial u_i}{\partial x_j} + \frac{\partial u_j}{\partial x_i} - \frac{2}{3}\delta_i \frac{\partial u_i}{\partial x_j}\right) + \frac{\partial}{\partial x_j}\left(-\rho\overline{u_i' u_j}\right)\right] \tag{1.16}$$

$$\frac{\partial}{\partial t}(\rho E) + \frac{\partial}{\partial x_i}[u_i(\rho E + p)] = -\frac{\partial}{\partial x_j}\left[\left(k + \frac{C_p \mu_t}{0.85}\right)\frac{\partial T}{\partial x_j}\right] + u_i\left(-\rho\overline{u_i' u_j'}\right) \tag{1.17}$$

where:
- u_i' and u_j' are the velocity fluctuations in the *i*-direction and *j*-direction,
- (μ) is the dynamic viscosity,
- $\rho\overline{u_i' u_j'}$ are the unknowns turbulent or Reynolds-stress tensors.

1.4.3 Turbulence modelling: the *k*-ω sst model

The governing equations (1.15, 1.16 and 1.17) are not a closed set and require turbulence closure models to express the Reynolds-stress tensors that would introduce additional equations 'approximating' the effects of turbulence on the mean flow. Several turbulence models are available for this purpose, and the present study applied the *k*-ω sst model (sst standing for shear stress transport). It is a two-equation model that is particularly effective in near-wall region flows where it accurately predicts the behavior of the boundary layer. It expresses the turbulent kinetic energy (k) and the specific dissipation rate (ω) [10]:

$$\frac{\partial}{\partial t}(\rho k) + \frac{\partial}{\partial x_i}(\rho k u_i) = \frac{\partial}{\partial x_j}\left(\Gamma_k \frac{\partial k}{\partial x_j}\right) + G_k - Y_k + S_k \tag{1.18}$$

$$\frac{\partial}{\partial t}(\rho \omega) + \frac{\partial}{\partial x_i}(\rho \omega u_i) = \frac{\partial}{\partial x_j}\left(\Gamma_\omega \frac{\partial \omega}{\partial x_j}\right) + G_\omega - Y_\omega + D_\omega + S_\omega \tag{1.19}$$

where (G_k) represents the mean velocity gradient turbulence kinetic energy production, (G_ω) indicates the specific rate of turbulence dissipation, (Γ_k) and (Γ_ω) act as (k) and (ω) effective diffusivities, (Y_k) and (Y_ω) as dissipation due to turbulence. Finally, (D_ω) that represents the cross-diffusion term while (S_k) and ($S\omega$) symbolize source terms usually defined by the user.

1.5 THE ISENTROPIC FLOW AND ITS DESCRIBING RELATIONSHIPS

An isentropic flow refers to a special type of steady, adiabatic, and reversible. It may be described by:

$$\Delta S = 0 \tag{1.20}$$

Where (S) represents the entropy, a thermodynamic property that measures the disorder in a system. In an isentropic process, the entropy remains constant.

The isentropic relationships are a set of equations that describe how various properties of a compressible fluid change when the flow is isentropic. They may be expressed as:

$$P\rho^{-\gamma} = \text{constant} \tag{1.21}$$

$$\frac{P_1}{P_2} = \left(\frac{\rho_1}{\rho_2}\right)^{\gamma} \tag{1.22}$$

$$\frac{T_1}{T_2} = \left(\frac{P_1}{P_2}\right)^{(\gamma-1)/\gamma} \tag{1.23}$$

$$\frac{T_1}{T_2} = \left(\frac{P_1}{P_2}\right)^{(\gamma-1)/\gamma} \tag{1.24}$$

$$\frac{p_0}{p} = \left(1 + \frac{\gamma-1}{2}M^2\right)^{\frac{\gamma}{\gamma-1}} \tag{1.25}$$

$$\frac{T_0}{T} = 1 + \frac{\gamma-1}{2}M^2 \tag{1.26}$$

1.6 THE PROPULSION NOZZLES

1.6.1 Early concepts and development of nozzles

The use of nozzle propulsion dates back to ancient Greece and China. In the 1st century AD, Hero of Alexandria described the aeolipile, a steam-powered device that used nozzle propulsion to create rotary motion. By the 9th century in China, gunpowder-propelled rockets were being developed, showcasing early applications of nozzle technology. During the medieval and Renaissance periods, nozzle propulsion saw further advancements, particularly with gunpowder rockets in China and the Islamic world. By the 13th century, these technologies had spread to Europe, marking a significant milestone in the history of propulsion. These early innovations laid the groundwork for the sophisticated propulsion systems seen today in modern aerospace engineering and rocketry [11].

Figure 1.2 gunpowder rockets

In the 17th century, Kazimierz Siemienowicz, a general in the Polish-Lithuanian Commonwealth, published 'The Complete Art of Artillery'. His work included designs for multi-stage rockets, laying the foundation for future rocket technology and space exploration.

The 19th century saw further advancements with British engineer Sir William Congreve design of the Congreve rocket, which enhanced stability and range with a guidance stick. These rockets were notably used during the War of 1812. The advancements of the 17th and 19th centuries paved the way for modern rocketry and space exploration [11].

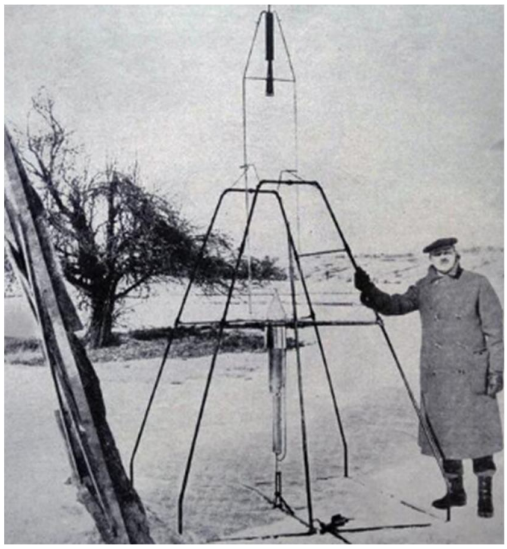

Figure 1.3 Early launching rocket (Robbert Goddal)

The modern era of rocketry began in the early 20th century. Visionaries like Konstantin Tsiolkovsky published seminal works in 1903 outlining the principles of space travel. In 1926, Robert Goddard launched the first successful liquid-fuel rocket, earning him the title 'father of modern rocketry'. During World War II, Nazi Germany's development of the V-1 and V-2 rockets, the latter being a long-range 'guided' ballistic missile using liquid propellants and turbo pumps and developed by the Wernher von Braun scientific team that later migrated to the u.s.a [12].

After World War II and during the Cold War era, the Soviet Union took an early lead with the launch of Sputnik-1 back in 1957. The United States caught up with the Mercury and Gemini programs, ultimately achieving the goal of landing humans on the moon with the Apollo program. Since then, rocket propulsion has continued to advance.

Figure 1.4 Baxter jet engine

In the early 20th century, pioneering engineers like Frank Whittle in the United Kingdom and Hans von Ohain in Germany independently developed the first operational jet engines, using centrifugal compressors and axial-flow turbines for thrust generation. In the modern era, significant advancements in materials science and engineering have propelled the evolution of jet engines.

One crucial innovation in nozzle design is due to French engineer Gustaf de Laval in the late 19th century. This convergent-divergent nozzle accelerates hot gases to supersonic speeds, which is essential for both rocket and jet engines. Modern jet engines often use variable-area nozzles that can adjust their shape to optimize performance across different flight conditions, enhancing fuel efficiency and thrust. All these advancements in nozzle design have been critical to the development of modern jet engines, enabling higher efficiencies and greater thrust, while also providing enhanced maneuverability for aircrafts.

1.6.2 Diverse profiles

The diverse nozzle profiles used in propulsion each have unique advantages and specific applications. From the simple conical nozzle to the advanced aerospike nozzle, the choice of nozzle profile plays a crucial role in the performance and efficiency of propulsion systems. Here, the main profiles are presented.

1.6.2.1 The conical nozzle

The simplest and earliest nozzle geometry is a cone (Figure 1.5). Although the exit velocity of the combustion gases from such a nozzle is essentially equal to its 1-D value corresponding to a given area ratio, the direction of the exit flow is not axial. This loss is accounted for by a factor (λ) expressed as:

$$\lambda = \frac{1+\cos(\alpha)}{2} \tag{1.27}$$

where: (α) is the divergence angle usually taken equal to 15°.

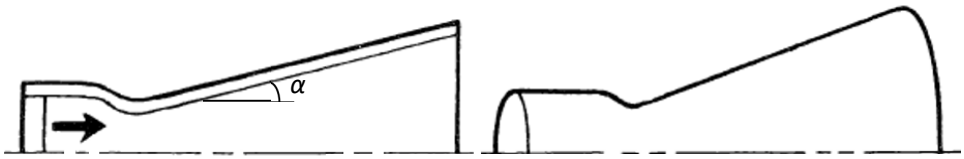

Figure 1.5 Conical nozzle

1.6.2.1 The contoured Nozzle or Bell Nozzle

The performance losses, particularly in terms of thrust, of the conical configuration due to divergence at the exit flow increase with the angle (α). A method to avoid this disadvantage is to 'turn' the divergent section inward as shown in Figure 1.6.

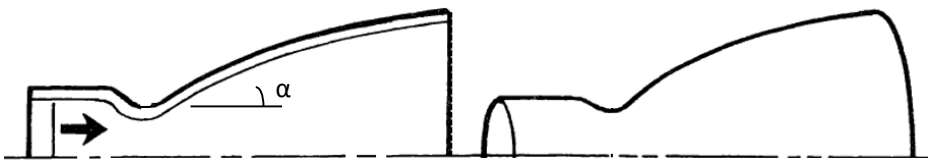

Figure 1.6 Contoured nozzle

In this case, a relatively large divergence angle near the throat can be used, allowing significant expansion. The second part of the divergent section, due to its curved shape, will tend to guide the flow in the axial direction, thus limiting the thrust losses due to divergence encountered with the conical nozzle.

1.6.2.3 The annular nozzle

Another type of nozzle widely used in turbomachines is called an annular nozzle. It has throat sections in the shape of a ring formed by a central 'plug' and an outer wall. Downstream of the throat, the exhaust gases undergo expansion in the divergent ring formed by the converging contour of the central plug and the divergent section of the nozzle (Figure 1.7). Its thrust is reduced by a factor (λ) relatively to a conical contour.

$$\lambda = \frac{\frac{1}{2}(sin\alpha+sin\beta)^2}{(\alpha+\beta)sin\beta+cos\beta-cos\alpha} \qquad (1.28)$$

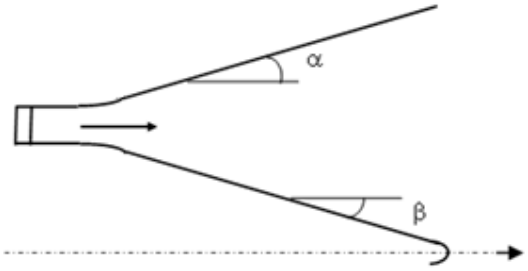

Figure 1.7 Annular nozzle

1.6.2.4 Self-adjusting nozzles

In the case of a self-adjusting nozzle, the expansion process is directly or indirectly regulated by the ambient pressure. The gas flow in this case adjusts itself to conform to external conditions. Two categories of this type of nozzles are used:

- The plug-type nozzles: The throat of this type of nozzle has the shape of a ring located at the outer diameter (Figure 1.8). The flow is controlled by expansion waves caused by the deflection of the plug, whose surface is the main influencing parameter.
- The Expansion-Deflection type Nozzles: This type of configuration is obtained through adding an obstacle such as the one described in Figure 1.9, which allows not only expansion but also deflection of the combustion gas flow.

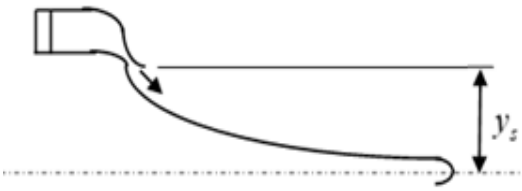

Figure 1.8 Plug-type nozzle

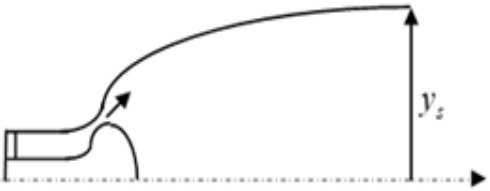

Figure 1.9 Expansion-Deflection nozzle

1.6.2.5 Dual-bell nozzles

Dual-bell nozzles incorporate two bell shapes to optimize performance at sea level and high altitudes. They have two distinct expansion sections: an inner bell for lower altitudes and an outer one for higher altitudes. A transition occurs between the two sections as the vehicle ascends. It allows for a wider operational range (Figure 1.10).

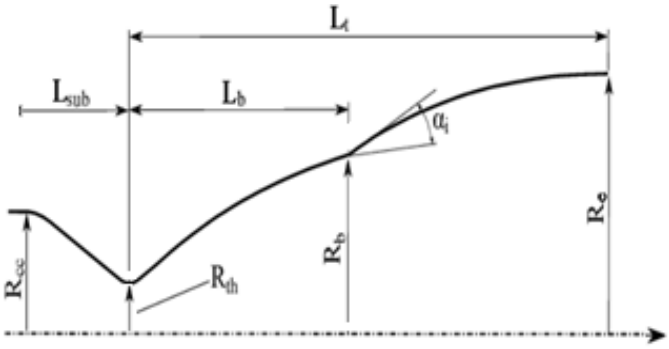

Figure 1.10 Dual-bell nozzle

1.6.3 Performance parameters of propulsion nozzles

Nozzle performance parameters are critical in determining the efficiency and effectiveness of propulsion systems across various aerospace and engineering applications, therefore making them essential in the design and optimization of nozzles. Key performance parameters include thrust coefficient, specific impulse, exit velocity, and flow characteristics such as pressure and temperature distributions.

1.6.3.1 The thrust, (T)

The thrust of a propulsion nozzle represents the conversion of thermal energy originating from the combustion chamber into kinetic energy at the exit section added to the difference of pressure between the exit and surroundings.

$$T = \dot{m}(V_{exit} - V_0) + (P_{exit} - P_{ambiant})A_{exit} \quad (1.28)$$

1.6.3.2 The effective velocity, (V_{eff})

The effective exhaust velocity reflects the efficiently the fuel is converted into thrust. It is expressed as the ratio of the thrust (T) to the mass flow rate ($\dot{m}$), providing a measure of fuel consumption efficiency.

$$V_{eff} = \frac{T}{\dot{m}} \quad (1.29)$$

1.6.3.3 The specific impulse, (I_{sp})

The specific impulse is defined as the ratio of the thrust to the product of the mass flow rate and the acceleration due to gravity. It is expressed as:

$$I_{sp} = \frac{T}{\dot{m}g} \quad (1.30)$$

1.6.3.4 The characteristic velocity, (c*)

The characteristic velocity of a reaction is defined as the ratio of the product of the total pressure by the throat area (A_t) to the mass flow rate:

$$c^* = \frac{P_t . A_t}{\dot{m}} \tag{1.31}$$

1.6.3.5 The thrust coefficient, (C_T)

The thrust coefficient is a dimensionless parameter defined as the ratio of the thrust to the product of the total or stagnation pressure to the throat area. It is a characteristic of the gas expansion in the divergent section of the nozzle, and may be considered representative of the performance of the supersonic divergent section contour.

$$c_T = \frac{T}{P_t . A_t} \tag{1.32}$$

1.6.3.6 The Discharge coefficient (C_d)

Due primarily to friction effects, the actual performance of a nozzle is generally different from that determined based on the assumption of isentropic flow. The discharge coefficient is defined as the ratio of the actual mass flow rate to that determined from isentropic relations.

$$C_d = \frac{\text{Débit actuel réel}}{\text{Débit isentropique}} \tag{1.33}$$

1.7 THE CONVERGENT-DIVERGENT (C-D) OR DE LAVAL NOZZLES

1.7.1 Principle and constituting sections

Convergent-divergent (C-D) nozzles, also known as de Laval nozzles, are designed to efficiently accelerate a fluid to supersonic speeds. The nozzle has a throat at the end of the convergent section, followed by a widening section or divergent section (Figure 1.11).

- Convergent section: As the fluid enters the convergent section, it is compressed, causing its velocity to increase and its pressure to decrease.
- Throat: At the narrowest point i.e. the throat, the fluid reaches its maximum subsonic speed (i.e. Mach equal unity). At that section, the velocity is at its highest and the pressure is at its lowest for subsonic flow.
- Divergent Section: After the throat, the nozzle widens. If the fluid has reached the speed of sound at the throat (Mach=1), it continues to accelerate in the divergent section, becoming supersonic. The pressure continues to decrease while the velocity increases.

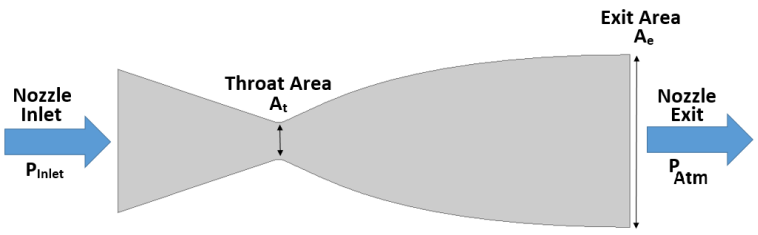

Figure 1.11 Convergent divergent (C-D) nozzle

1.7.2 Performance parameters

Under steady flow conditions, the mass flow rate through a nozzle is constant and can be expressed as:

$$\dot{m} = \rho \cdot V \cdot A = \frac{P \cdot A}{R \cdot T} \tag{1.34}$$

For an ideal gas, Equation 1.34 may be written as:

$$\dot{m} = \frac{P \cdot A}{\sqrt{\gamma \cdot R \cdot T}} M \tag{1.35}$$

The total and stagnation temperatures (T_0) and pressures (P_0) may be expressed in terms of the Mach number (M) for an isentropic flow:

$$T = T_0 \left(1 + \frac{\gamma - 1}{2} M^2\right)^{-1} \tag{1.36}$$

$$P = P_0 \left(1 + \frac{\gamma - 1}{2} M^2\right)^{-\frac{\gamma}{\gamma - 1}} \tag{1.37}$$

Finally, the mass flow rate can be expressed:

$$\dot{m} = \frac{P_0 A}{\sqrt{\gamma R T_0}} M \left(1 + \frac{\gamma - 1}{2} M^2\right)^{-\frac{\gamma + 1}{2(\gamma - 1)}} \tag{1.38}$$

For specified stagnation temperature and pressure, and for a defined cross-section area, the maximum mass flow rate occurs at M=1 at the throat (chocked condition):

$$\dot{m}_{\max} = \frac{P_0 A}{\sqrt{\gamma R T_0}} \left(1 + \frac{\gamma - 1}{2}\right)^{-\frac{\gamma + 1}{2(\gamma - 1)}} \tag{1.39}$$

Table 1.1 Properties of compressible flow of a perfect gas with γ=1.4 [13]

M	P/P_t	ρ/ρ_t	T/T_t	S/S^*
0.0	1.0000	1.0000	1.0000	∞
0.2	0.9725	0.9803	0.9921	2.9630
0.4	0.8956	0.9243	0.9690	1.5901
0.6	0.7840	0.8405	0.9328	1.1882
0.8	0.6560	0.7400	0.8865	1.0382
1.0	0.5283	0.6339	0.8333	1.000
2.0	0.1278	0.2300	0.5556	1.688
3.0	0.02722	0.07623	0.3571	4.235
4.0	0.006586	0.02766	0.2381	10.72
5.0	0.001890	0.01134	0.1667	25.00
6.0	0.006334	0.005194	0.1220	53.18
7.0	0.0002416	0.002609	0.09259	104.1
8.0	0.0001024	0.001414	0.07246	190.1
9.0	0.00004739	0.0008150	0.05814	327.2
10.0	0.00002356	0.0004948	0.04762	535.9
0.0	1.0000	1.0000	1.0000	∞

The preceding equations 1.38 and 1.39 provide a relationship linking the variation of any cross-section area to that at the throat:

$$\left(\frac{S_1}{S_2}\right)_M = \left(\frac{\gamma+1}{2}\right)^{\frac{1}{\gamma-1}} \left(\frac{1+\frac{\gamma-1}{2}M^2}{\frac{\gamma+1}{2}}\right)^{\frac{\gamma+1}{2(\gamma-1)}} \tag{1.40}$$

The various properties of an isentropic 1-D compressible flow may then be expressed as function of the Mach number. An overview of these data is presented in Table1.1.

1.8 THE CHARACTERISTIC APPROACH: THE METHOD OF CHARACTERISTICS (MoC)

1.8.1 Introduction to MoC

The physical conditions of a 2-D, steady, isentropic, irrotational flow can be expressed mathematically by the nonlinear differential equation of the velocity potential [14-15]. The MoC is a computational approach that simplifies the resolution of Partial Differential Equations (PDEs) by converting them into a set of Ordinary Differential Equations (ODEs). This conversion is valid in scenarios where the PDEs are applicable along specific trajectories known as characteristic curves. The key idea behind the MOC is that changes in fluid properties within supersonic flows occur along these characteristic curves due to pressure waves propagating along the Mach lines. These Mach lines are angled at the Mach angle relative to the local velocity vectors. The MOC's capacity to yield accurate solutions for challenges in supersonic flow renders it a pivotal method in the realms of fluid dynamics and aeronautical engineering [16].

1.8.2 Basic characteristics of MoC

Assuming the flow is isentropic, 2-D, non-viscous, and irrotational, the equations describing the flow taking place within a supersonic nozzle can be expressed by:

$$(u^2 - a^2)\frac{\partial u}{\partial x} + (v^2 - a^2)\frac{\partial v}{\partial y} + 2uv\frac{\partial u}{\partial y} - \delta\frac{a^2 v}{y} = 0 \tag{1.41}$$

$$\frac{\partial u}{\partial y} - \frac{\partial v}{\partial x} = 0 \tag{1.42}$$

$$a = a(u, v) \tag{1.43}$$

The characteristic and compatibility equations, Equations 1.44 and 1.45 respectively, derived from the governing equations are obtained [17] and are solved along the characteristics or Mach lines represented in Figure 1.12:

$$\lambda_{\pm} = \left.\frac{dy}{dx}\right|_{\pm} = \frac{uv \pm a^2\sqrt{M^2-1}}{u^2-a^2} = \mathrm{tg}(\theta \pm \alpha) \tag{1.44}$$

$$(u^2 - a^2)du_{\pm} + [-(u^2 - a^2)\lambda_{\pm} + 2uv]dv_{\pm} - \left(\delta\frac{a^2 v}{y}\right)dx_{\pm} = 0 \tag{1.45}$$

The compatibility equation (1.45) provides two differential equations linking the components of velocity (u) and (v). It is valid only along the characteristic lines C_+ and C_- defined by the characteristic equation (1.44).

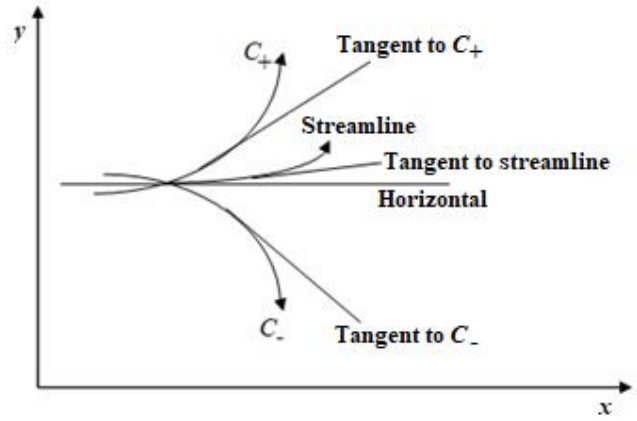

Figure 1.12 Representation of the characteristics C_+ and C_- (Mach lines)

The characteristic and compatibility relationships (1.14 and 1.15) are solved through the application of the finite difference method (FDM), a numerical technique used to solve differential equations by approximating them with difference equations. In order to achieve that, the derivatives in the differential equations are replaced with finite difference approximations, which involve the values of the function at specific discrete points. The key advantage of FDM is its simplicity and ease of implementation, making it a popular choice for solving problems on computational grids.

1.9 THE FINITE VOLUME METHOD: ANSYS-FLUENT PLATFORM

'ANSYS Fluent' is a widely utilized CFD software tool for simulating various fluid flow phenomena, including supersonic steady turbulent viscous flows. 'Fluent' provides a robust and versatile environment for modeling, simulating, analyzing, and visualizing complex fluid flow behaviors.

The Finite Volume Method (FVM) is a numerical technique used for solving partial differential equations, especially those arising from fluid dynamics problems. It is widely adopted in computational fluid dynamics (CFD) due to its ability to conserve quantities like mass, momentum, and energy within a discretized domain. In steady viscous turbulent supersonic flow simulations like those in this study, 'ANSYS Fluent' solves the core governing equations of fluid dynamics and turbulence modeling. These include (1) the continuity equation, the momentum conservation or Navier-Stokes equations, and the energy conservation equation. The system is closed through a modeling of the turbulence. In the present case, the model applied is represented by the RANS equations with sst k-ω turbulence closure model.

'ANSYS Fluent' is structured into various modules, each serving a specific function within the simulation process. The primary modules are represented by the:

- 'Preprocessing' that integrates geometry modeling and meshing.
- 'Solver Setup' involving defining boundary conditions such as inlet, outlet, and wall conditions that may be selected by the user.
- 'Solution' where the simulation based on the defined setup is initiated, iteratively solving the governing equations until convergence.

- 'Post-Processing' which provides visualization tools for creating contour plots, vector plots, animations, streamlines …etc.
- 'Additional modules' that include multiphase modeling, combustion modeling … etc. that are applied in the present simulations.

1.10 CONCLUSION

The present chapter has established the theoretical and numerical foundations necessary for understanding supersonic flows, designing C-D nozzles and solving the governing equations that describe these flows through application of MoC and Ansys-Fluent.

Chapitre2:

THE DESIGN APPROACH PROCEDURE – MoC

2.1 GENERAL

This chapter will be dedicated to the application of the Method of Characteristics (MoC) for designing divergent profiles of de-Laval supersonic nozzles. A program using the Fortran language will be utilized for this purpose, with the goal of designing the divergent sections of three nozzles. The first, conical in shape, will be approximated by a straight-line. The second, with a contour profile, will be approximated by a second-degree polynomial while the third and last, referred to as open, will be approximated by an exponential.

2.2 THE CONICAL NOZZLE

For a conical nozzle, the profile of the divergent section can be described by a linear equation (Figure 2.1):

$$y = A_w + B_w x \tag{2.1}$$

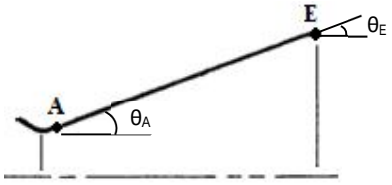

Figure 2.1 Conical nozzle divergent section

with the boundary conditions:

$$y_A = A_w + B_w x_A \tag{2.2}$$

$$\left(\frac{\partial y}{\partial x}\right)_A = B_w = \tan\theta_A = \tan\ \theta_E \tag{2.3}$$

The constants (A_w) and (B_w) are obtained by applying the relationships that connect the attachment point (A) to the upstream circular arc of the throat i.e.:

$$B_w = \tan\theta_A \tag{2.4}$$

$$A_w = y_A - x_A \cdot tan\,\theta_A \tag{2.5}$$

The application of the method of characteristics requires the input data represented in Table 2.1. The results provided by the Fortran program integrating the MoC for the conical profile are summarized in Table 2.2.

Table 2.1 Input data for the calculation using the MoC

P_t (bar)	54
T_t (K)	2500
P_a (bar)	1.013
y_t (m)	0.088
R_{tu} (m)	0.176
R_{td} (m)	0.044
Y_e (m)	0.197
Θ (°)	10

Table 2.2 Geometric results of the calculations using the MoC

x_e (m)	0.62202
x_A (m)	0.00764
y_A (m)	0.08870
A_w	0.08732
B_w	0.17633

The results obtained allow for the definition of the supersonic profile through the expression of the arc of the circle and the straight line describing it. A cloud of points is created, with a step of 0.001m, describing:

- The arc-of-circle downstream of the throat:

$$x^2 + (y + R_{td} - y_E)^2 = R_{td}^2 \quad \text{with} \quad x \in [0, x_A = 0.00764m] \tag{2.6}$$

$$y = \sqrt{R_{td}^2 - x^2} - R_{td} + y_t \tag{2.7}$$

- The straight line that would be linked to the arc above at the attachment point:

$$y = A_w + B_w x \quad \text{with} \quad x \in [x_A = 0.00764m\,, x_e = 0.62202m] \tag{2.1}$$

The results are shown in Table 2.3 and Figure 2.2 for the arc-of-circle , and Table 2.4 and Figure 2.3 for the straight line representing the conical nozzle.

Table 2.3 Describing points of the arc-of-circle downstream of the throat

x (m)	y (m)
0	0,088
0,001	0,08801137
0,002	0,08804548
0,003	0,08810239
0,004	0,0881822
0,005	0,08828501
0,006	0,08841101
0,007	0,08856039
0,00764	0,08866837

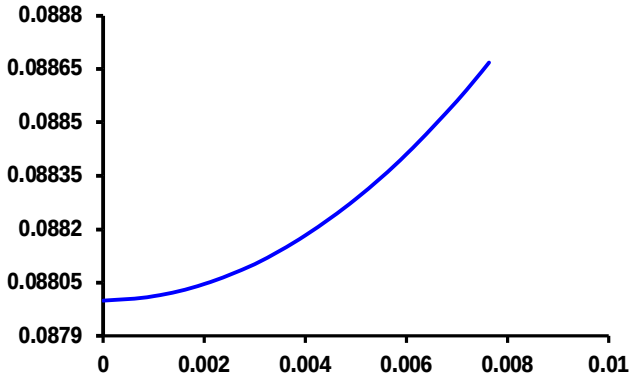

Figure 2.2 Conical nozzle arc-of-circle

Table 2.4 Describing points of the straight line

x (m)	*y* (m)
0.10764	0.10630212
0.15764	0.11511847
0.20764	0.12393482
0.25764	0.13275117
0.30764	0.14156752
0.35764	0.15038387
0.40764	0.15920022
0.45764	0.16801657
0.50764	0.17683291
0.55764	0.18564926
0.60764	0.19446561
0.62202	0.19700119

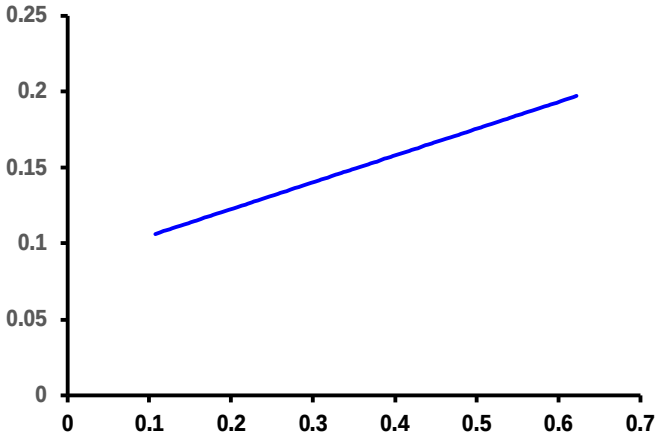

Figure 2.3 Conical nozzle straight line

The above computations and profiles led to the divergent section conical nozzle contour. Moreover, the characteristics may be built showing the mesh resulting from the application of the MoC (Figure 2.4).

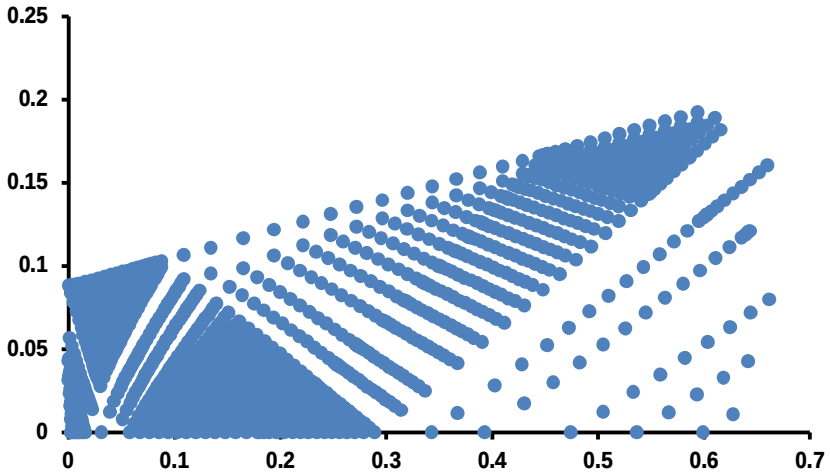

Figure 2.4 Supersonic section structured mesh grid topology of the conical nozzle

2.3 THE CONTOURED NOZZLE

For the contoured nozzle, the profile of the divergent section is simulated by a 2nd-degree polynomial of the form (Figure 2.5):

$$y = A_w + B_w x + C_w x^2 \tag{2.8}$$

Four unknowns are present within the equation: the constants (A_w, B_w, C_w) and length (x_e). Their determination needs four equations represented by the relationships describing the profile and its derivative at both the attachment point (A) and exit point (E):

$$y_A = A_w + B_w x_A + C_w x_A^2 \quad (2.9)$$

$$\left(\frac{\partial y}{dx}\right)_A = \tan\theta_A = B_w + 2C_w x_A \quad (2.10)$$

$$y_E = A_w + B_w x_E + C_w x_E^2 \quad (2.11)$$

$$\left(\frac{\partial y}{\partial x}\right)_E = \tan\theta_E = A_w + 2C_w x_E \quad (2.12)$$

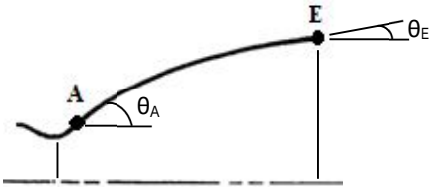

Figure 2.5 Contour nozzle divergent section

The combination of Equations 2.9, 2.10, 2.11 and 2.12 leads to:

$$C_w = \frac{\tan\theta_A - \tan\theta_E}{2(x_A - x_E)} \quad (2.13)$$

$$B_w = \frac{x_A \tan\theta_E - x_E tan\,\theta_A}{(x_A - x_E)} \quad (2.14)$$

$$A_w = y_A - \frac{x_A^2 \tan\theta_E + x_A^2 \tan\theta - 2x_A x_E \tan\theta_A}{2(x_A - x_E)} \quad (2.15)$$

$$x_e = \frac{\tan\theta_E - A_w}{2C_w} \quad (2.16)$$

The application of the method of characteristics utilizes the input data represented in Table 2.5. The results provided by the Fortran program integrating the MoC for the conical profile are summarized in Table 2.6.

Table 2.5 Input data for the calculation using the MoC

P_t (bar)	54
T_t (K)	2500
P_a (bar)	1.013
y_t (m)	0.088
R_{tu} (m)	0.176
R_{td} (m)	0.044
Y_e (m)	0.197
Θ_A (°)	20
Θ_E (°)	5

Table 2.6 Geometric results of the calculations using the MoC

x_e (m)	0.486
x_A (m)	0.01505
y_A (m)	0.09065
A_w	0.08511
B_w	0.37280
C_w	-0.29354

The results obtained allow for the definition of the supersonic contour through the expression of the arc of the circle and the contoured profile describing it. A cloud of points is

created, with a step of 0.001m, describing the same arc-of-circle downstream of the throat as expressed by Equations 2.6 and 2.7, but in this case with x_A = 0.01505m.

- The contoured profile that would be linked to the arc above at the attachment point:

$$y = A_w + B_w x \quad (2.8)$$

In this case: $x \in [x_A = 0.01505m\ , x_e = 0.486m]$

The results are shown in Table 2.7 and Figure 2.6 for the contour representing the contoured nozzle.

Table 2.7 Describing points of the contoured profile

x (m)	y (m)
0	0.088
0.002	0.08804548
0.004	0.0881822
0.007	0.08856039
0.008	0.08873339
0.01	0.08915143
0.011	0.08939718
0.012	0.08966798
0.013	0.0899643
0.014	0.09028669
0.01505	0.09065
0.018	0.09172529
0.1	0.1194546
0.25	0.15996375
0.486	0.197

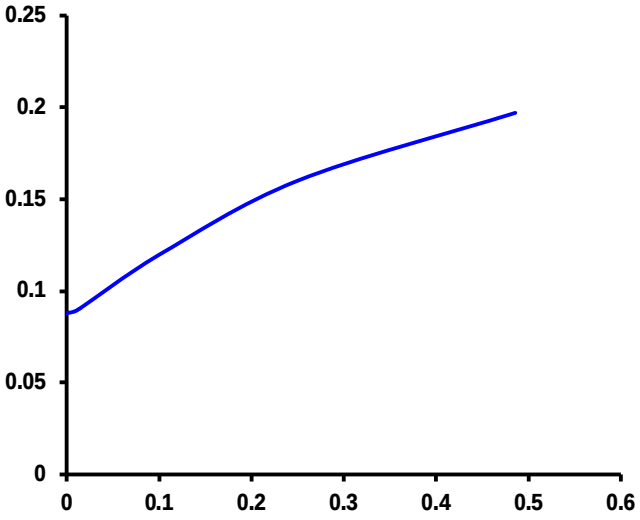

Figure 2.6 Contoured nozzle divergent section

The above computations and profiles led to the divergent section contoured nozzle contour. Moreover, the characteristics may be built showing the mesh resulting from the application of the MoC (Figure 2.7).

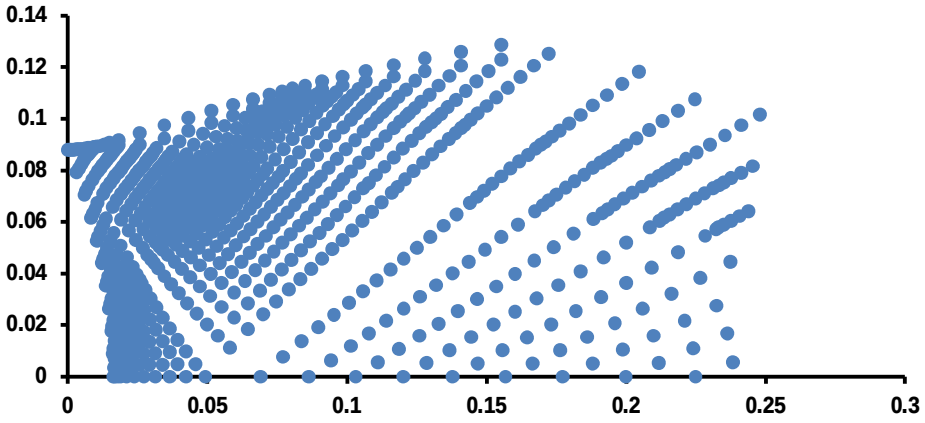

Figure 2.7 Supersonic section structured mesh grid topology of the contoured nozzle

2.4 THE OPEN NOZZLE

For the Case of the open nozzle, the profile of the divergent section is simulated by an exponential form (Figure 2.8):

$$y = A_w e^{B_w \cdot (x)} \tag{2.17}$$

Two unknowns (A_w and B_w) should be determined. Therefore, two equations are needed that involve the attachment point.

$$y_A = A_w + e^{B_w \cdot (x_A)} \tag{2.18}$$

$$\left(\frac{\partial y}{dx}\right)_A = \tan\theta_A = A_\omega B_w e^{B_w \cdot (x_A)} \tag{2.19}$$

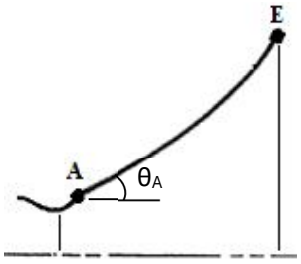

Figure 2.8 Open nozzle divergent section

The combination of Equations 2.18 and 2.19 leads to:

$$B_w = \frac{\tan\theta_A}{y_A} \tag{2.20}$$

$$A_w = exp\left[Ln(y_A) - \frac{x_A \cdot tg(\theta_A)}{y_A}\right] \tag{2.21}$$

The application of the method of characteristics utilizes the input data represented in Table 2.8. The results provided by the Fortran program integrating the MoC for the conical profile are summarized in Table 2.9.

Table 2.8 Input data for the calculation using the MoC

P_t (bar)	54
T_t (K)	2500
P_a (bar)	1.013
y_t (m)	0.088
R_{tu} (m)	0.176
R_{td} (m)	0.044
Y_e (m)	0.197
Θ_A (°)	15

Table 2.9 Geometric results of the calculations using the MoC

x_e (m)	0.26979
x_A (m)	0.01139
y_A (m)	0.08950
A_w	0.08650
B_w	2.99387

The same procedure applied in the conical and contoured cases is followed for the present open configuration. This would result in definition of the supersonic contour represented in Table 2.10 and the final profile in Figure 2.9.

Table 2.10 Describing points of the open profile

x (m)	*y* (m)
0	0.088
0.001	0.08801137
0.002	0.08804548
0.003	0.08810239
0.004	0.0881822
0.005	0.08828501
0.006	0.08841101
0.007	0.08856039
0.008	0.08873338
0.009	0.08893029
0.01139	0.08949979
0.10139	0.11717785
0.15139	0.13609952
0.20139	0.15807663
0.25139	0.18360255
0.26979	0.197

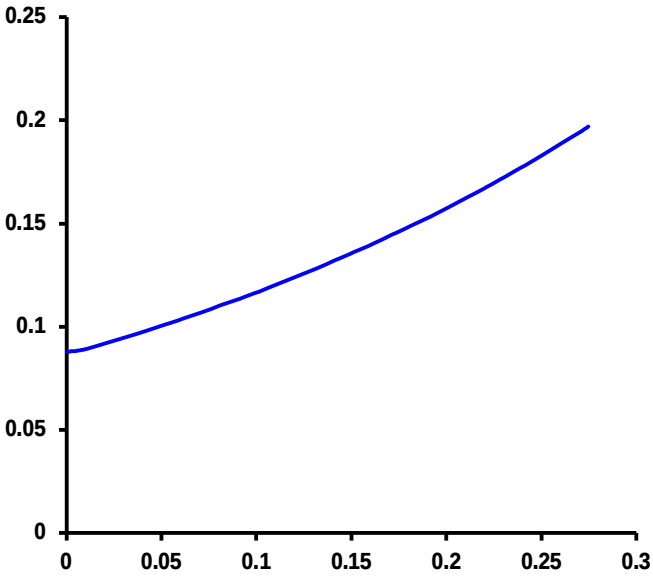

Figure 2.9 Open nozzle contour

The above computations and profiles led to the divergent section contoured nozzle contour. Moreover, the characteristics may be built showing the mesh resulting from the application of the MoC (Figure 2.10).

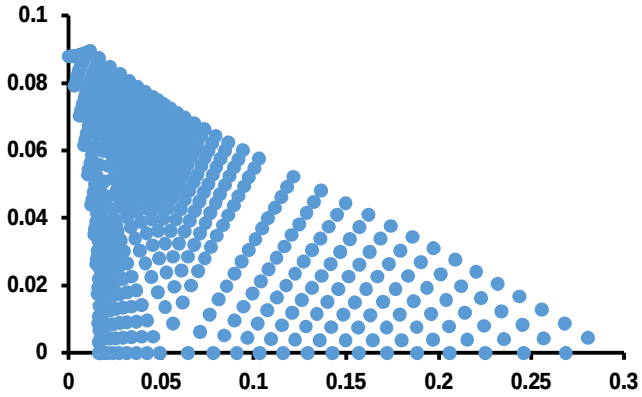

Figure 2.10 Supersonic section structured mesh grid topology of the open nozzle

2.5 THE CONVERENT SECTION

The convergent section has to lead the flow to reach transonic velocities at the throat. This would generate a supersonic expansion after the throat in the divergent. The convergent is produced by application of the Rao method [18] , an experimental procedure based on the throat radius (y_t). It expresses the convergent profile as:

$$x = 1{,}5 \cdot y_t \cdot \cos\theta \quad (2.22)$$

$$y = 1{,}5 \cdot y_t \cdot \sin\theta + 2{,}5y_t \quad (2.23)$$

with: $-130° \leq \theta \leq -90°$

As the convergent is common to all the profiles, the same results are applied for the conical, contour and open configurations. The resulting points constituting the profile and its representation are shown in Table 2.11 and Figure 2.11.

Table 2.11 Describing points of the convergent Section of all the nozzles

θ (°)	x (m)	y (m)
-130	-0.084847	0.11888
-128	-0.08126	0.11598
-126	-0.07758	0.113209
-124	-0.073813	0.110567
-122	-0.06994	0.108057
-120	-0.066000	0.105684
-118	-0.061970	0.103450
-116	-0.057864	0.101359
-114	-0.053689	0.099412
-112	-0.049448	0.097611
-110	-0.045146	0.099596
-108	-0.040790	0.099446
-106	-0.036384	0.093113
-104	-0.031933	0.091920
-102	-0.027444	0.090884
-100	-0.022921	0.090005
-98	-0.018370	0.089284
-96	-0.013797	0.088872
-94	-0.009207	0.088832
-92	-0.004606	0.088808
-90	8.086E-18	0.088000

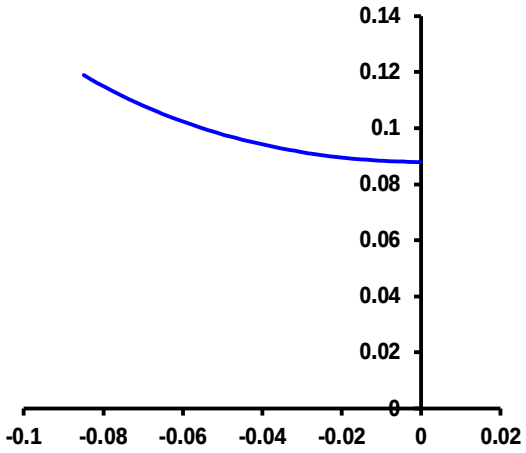

Figure 2.11 Convergent section contour

Finally, the complete profiles of the three nozzle configurations may be drawn (Figure 2.12). They will be integrated into the Fluent software in order to simulate the flow fields that would take place within the convergent, throat and divergent sections.

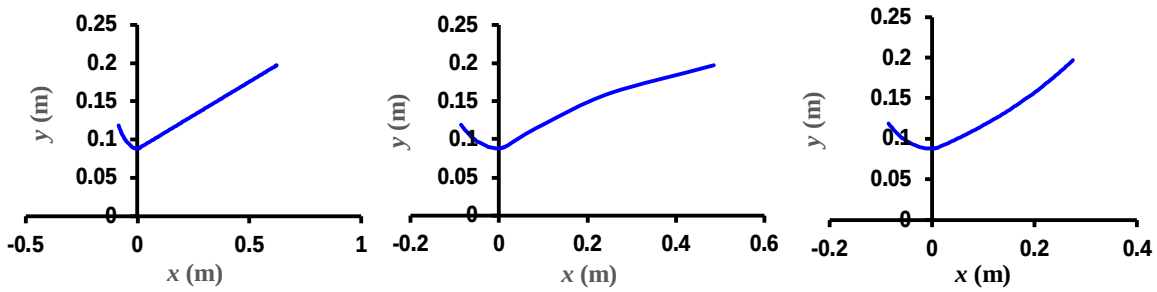

Figure 2.12 Nozzle three configurations: conical, contour and open

2.6 CONCLUSION

The present chapter applied the Method of Characteristics to design the profiles of three supersonic nozzles sections. Moreover, the convergent sections have been developed using the method of Rao [18]. The approach followed showed proof of the capabilities to end up with efficient nozzle profiles.

Chapitre3:

ANALYSIS OF THE DESIGNED PROFILES - ANSYS-FLUENT

3.1 GENERAL

In the present chapter, the analysis of the three configurations designed within chapter 2 is carried out. The platform 'Ansys-Fluent' is used to simulate the flow fields within the entire nozzles. The conservation of mass and energy are applied along with the RANS equations. The system is closed through applying the sst k-ω turbulence model.

The application of CFD software 'Workbench' platform in 'ANSYS-Fluent' leads to the interfaces and tools necessary to define, solve, and analyze the simulation that includes:

- Building the geometry,
- Generating the mesh,
- Integrating boundary conditions,
- Configuring and executing the simulation,
- Presenting the results.

3.2 THE CONICAL PROFILE C-D NOZZLE

The compressible expansion within the conical configuration was simulated using the CFD solver based on the finite volume method (ANSYS-Fluent). A mesh consisting of 3,600 elements (3782 nodes), 120 in the axial direction (x) and 30 in the radial direction (y), was generated. In areas near the throat, where property gradients are expected to be larger, and along the solid wall, where viscosity effects are significant, a more refined mesh was employed (Figure 3.1). Computations were carried out until optimal design conditions were achieved.

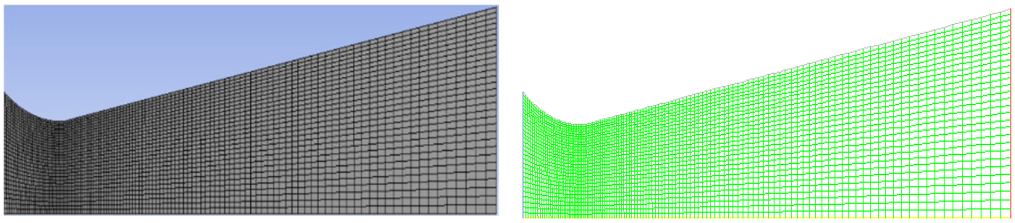

Figure 3.1 Conical nozzle grid topology

The governing equations representing the physical laws related to the conservation of mass, momentum, and energy are applied. These equations are used as the primary governing equations for the turbulent viscous flow field. The system of equations is closed using the k-ω sst model. The computational parameters used for the simulation are detailed in Table 3.1.

Table 3.1: Conical nozzle simulation settings

	Applied features
Model	2D, , stationary, viscous with compressibility effects
Solver	Density based
Turbulence model	*k-ω sst*
Fluid	air, ideal gas
Inlet Boundary Conditions	54.10^5 Pa / 2500 K
Outlet Boundary Conditions	$1.013.10^5$ Pa
Residual	10^{-6}

The iterations required for the computations to converge are illustrated in Figure 3.2. In this case, as specified in Table 3.1, the residual was set to (10^{-6}) which represents a stringent condition. Approximately 490 iterations were needed to achieve the desired solution. This solution, in the context of the RANS equations, is represented by the difference between the left and right sides of the equations, scaled to enhance interpretability and independence from the problem's magnitude.

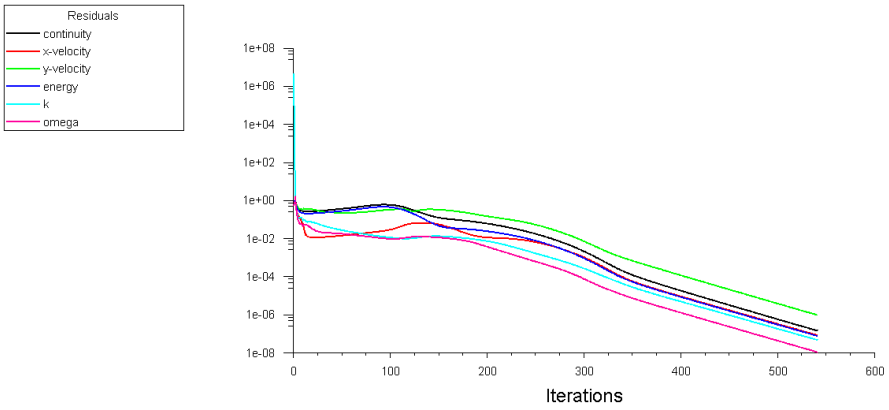

Figure 3.2 Scaled residuals of the conical flow-field computations using *k-ω* sst turbulence model

3.3 THE CONTOUR PROFILE C-D NOZZLE

The present study being focused on the impact of the nozzle profile on flow parameters and performance, the input data and boundary conditions are maintained the same for all three configurations. However, for the contoured configuration, the grid topology and therefore the convergence may differ.

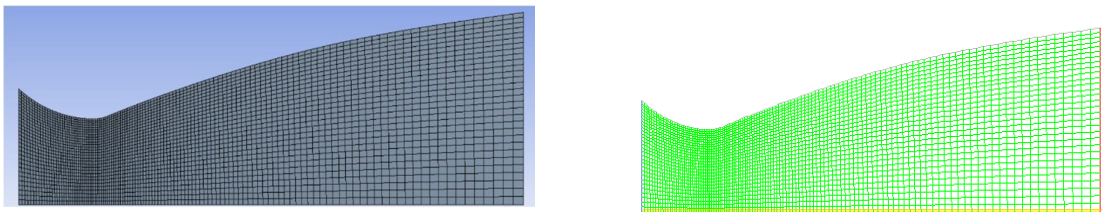

Figure 3.3 Contour nozzle grid topology

In the case of the contoured configuration, a mesh consisting of 3,600 elements (3,750 nodes), 120 in the axial direction (x) and 30 in the radial direction (y), was generated. In areas near the throat, where property gradients are expected to be larger, and along the solid wall, where viscosity effects are significant, a more refined mesh was employed (Figure 3.3). Computations were carried out until optimal design conditions were achieved.

The iterations required for the computations to converge are illustrated in Figure 3.4. In this case, as specified in Table 3.1, the residual was set to (10^{-6}) which represents a stringent condition. Approximately 220 iterations were needed to achieve the desired solution.

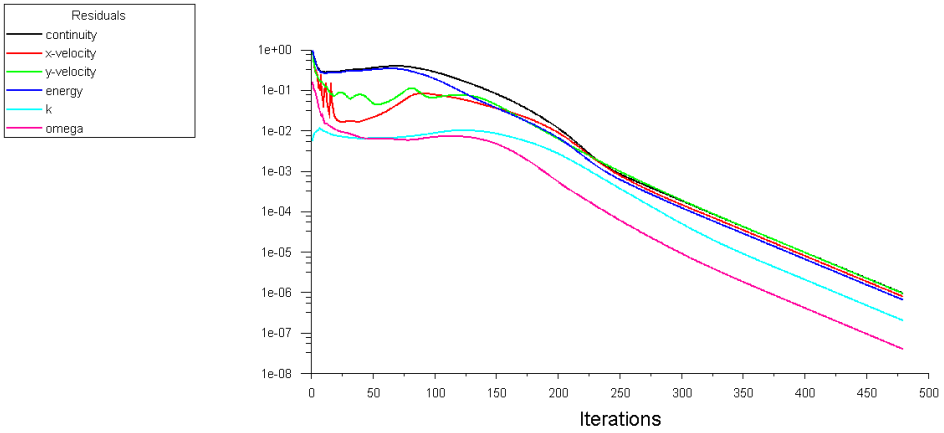

Figure 3.4 Scaled residuals of the contour flow-field computations using k-ω sst turbulence model

3.4 THE OPEN PROFILE C-D NOZZLE

As stated above (section 3.3), The input data and boundary conditions are maintained the same for all three configurations. However, for the open configuration, the grid topology and therefore the convergence may differ.

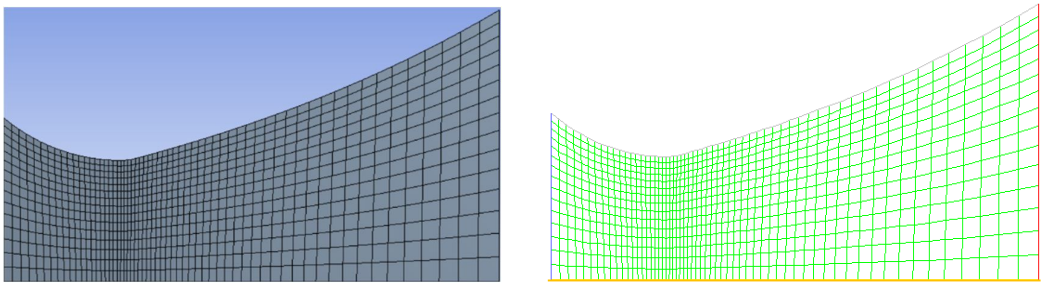

Figure 3.5 Contour nozzle grid topology

In the case of the open configuration, a mesh consisting of 3,600 elements (3,750 nodes), 120 in the axial direction (x) and 30 in the radial direction (y), was generated. In areas near the throat, where property gradients are expected to be larger, and along the solid wall, where viscosity effects are significant, a more refined mesh was employed (Figure 3.5). Computations were carried out until optimal design conditions were achieved.

The iterations required for the computations to converge are illustrated in Figure 3.6. In this case, as specified in Table 3.1, the residual was set to (10^{-6}) which represents a stringent condition. Approximately 520 iterations were needed to achieve the desired solution.

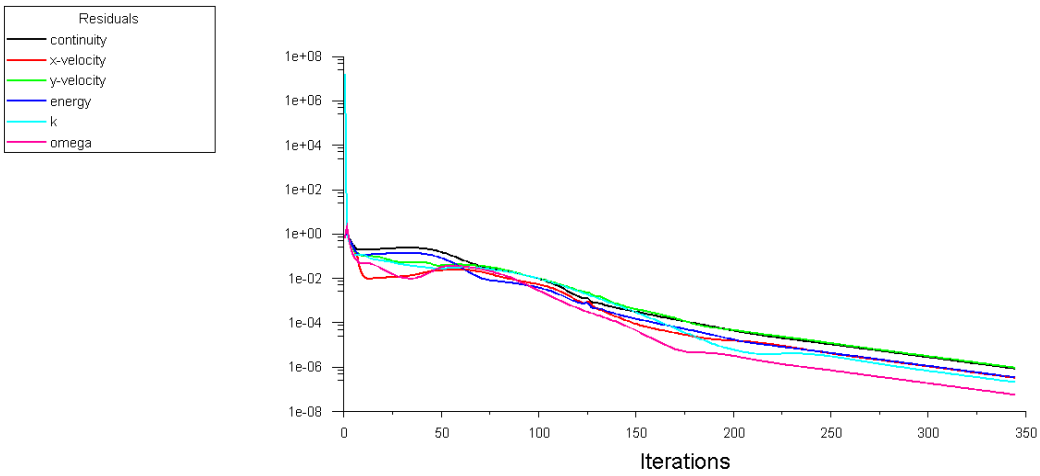

Figure 3.6 Scaled residuals of the open flow-field computations using *k-ω* sst turbulence model

3.5 CONCLUSION

This chapter introduced the simulation performed on the flow fields of the three configurations using the 'Ansys-Fluent' platform. The grids have been put in place for the three geometries, and the computations performed. All the simulations used the sst *k-ω* model of turbulence, and have converged successfully. The results obtained along with their comparisons are carried out in the following chapter 4.

Chapitre4:
RESULTS AND DISCUSSION

4.1 GENERAL

The analysis and comparisons, in terms of performance parameters, are carried out within the present chapter. The simulations have been performed in 2-D, and focus is turned towards pressure and Mach distributions along centerline and wall within the three configurations. The performance parameters comprise essentially the thrust, the coefficient of thrust, the mass flow rate, the specific impulse, the effective velocity and the Mach at exit.

4.2 THE CONICAL PROFILE C-D NOZZLE

4.2.1 Pressure and Mach profiles

Figure 4.1 displays the pressure distribution along the centerline and wall of the conical configuration. It shows a rapid decrease in pressure along both the axis and the wall, that along the wall being a bit higher. Towards the exit, the two curves converge. In terms of Mach number (Figure 4.2), the Mach number is almost null at the entrance low i.e. x/y_t close to (-1) that is immediately at the combustion chamber exit. Afterwards, the Mach starts its increase to reach approximately 3.12 at the centerline and 2.34 at the wall. The steady increase in Mach along the nozzle indicates a progressive acceleration of the flow resulting from an expansion of the gases. The difference, in terms of Mach, between centerline and wall is mainly due to the friction, and this is typical for flow fields with solid boundaries such as nozzles.

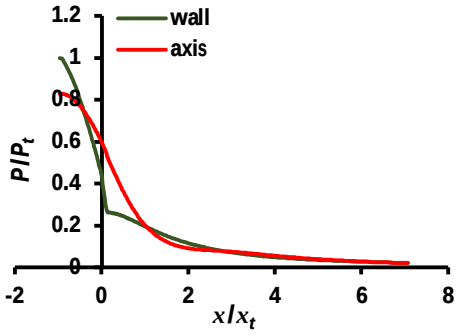

Figure 4.1 Conical nozzle: Pressure distributions along centerline and wall

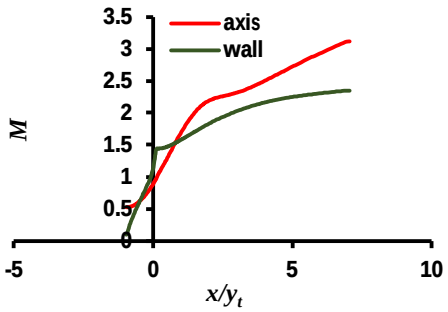

Figure 4.2 Conical nozzle: Mach distributions along centerline and wall

4.2.2 Pressure and Mach contours

The same results noticed in terms of profiles are repeated in the contours. The expansion starts from the entrance i.e. at the beginning of the subsonic section until the exit of the nozzle (Figure 4.3). Maily due to the 10° angle of divergence, the pressure transition is relatively

smooth and linear. In contrast, the Mach number increases with the decrease of the pressure (Figure 4.4). The relatively long length of the nozzle allows for a gradual expansion of the gases, contributing to a uniform decrease in pressure. This design is ideal for applications requiring flow stability and a gradual reduction in pressure.

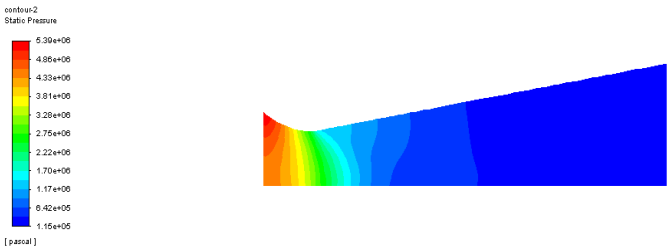

Figure 4.3 Conical nozzle: Pressure contour

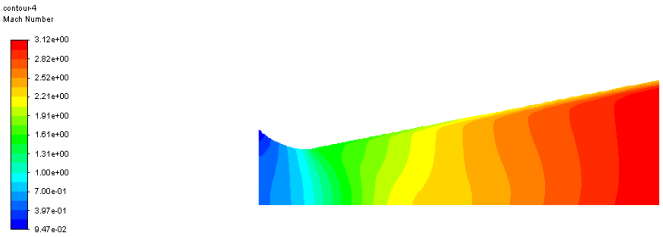

Figure 4.4 Conical nozzle: Mach contour

4.2.3 Velocity contour distributions

Figure 4.5 illustrates the velocity distribution along the entire length of the nozzle. A progressive but continuous and uniform increase may be noted beginning at the entry until the exit. Figure 4.6 shows the velocity distributions at cross-sections along the nozzle. The uniformity of the expansion is noticed as well as the continuous acceleration of the flow.

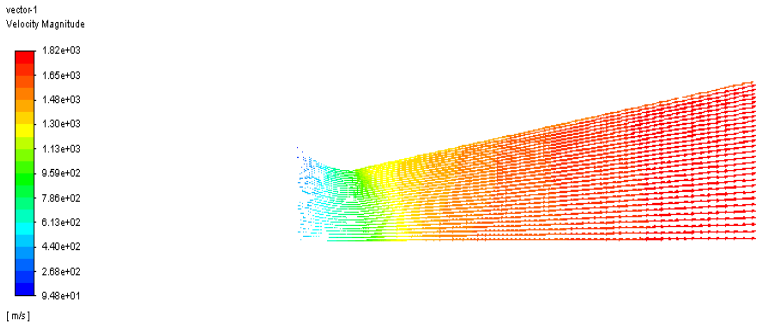

Figure 4.5: Velocity distribution along conical nozzle

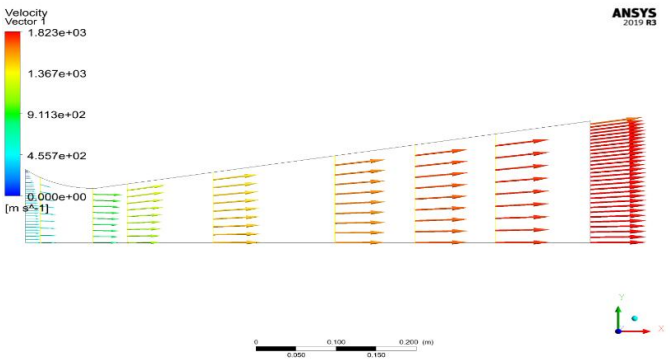

Figure 4.6: Velocity distribution along cross-sections of conical nozzle

4.2.4 Performance parameters

The performance parameters of the contour nozzle are determined using the relationships derived in Section 1.6.3, and are presented in Table 4.1. The results obtained will be later compared to those gathered for the two other configurations i.e. contour and open.

Table 4.1: Conical nozzle performance parameters

Performance parameters	Conical nozzle
Thrust, T (N)	279,203.67
Mass flow rate, $\dot{m}$ (kg/s)	170.78
Thrust coefficient, C_T (-)	2.12
Specific impulse, I_s (s)	166.65
Effective velocity, V_{eff} (m/s)	1634.80
M_{exit}	2.34

4.3 THE CONTOUR PROFILE C-D NOZZLE

4.3.1 Pressure and Mach profiles

Figure 4.7 illustrates the pressure distribution along the centerline and wall of the contoured configuration. A fast pressure drop along both the axis and wall are represented, with a convergence of both profiles at the exit. Regarding the Mach number (Figure 4.8), it is nearly zero at the entrance but starts increasing along the nozzle, reaching approximately 3.5 at the centerline and 2.33 at the wall. This increase in Mach is found to be faster at the beginning due to the 20° attachment angle, but starts increasing in a slower manner afterwards probably due to friction effects at the wall and the contour profile of the divergent configuration that reaches a 5° angle at the exit.

The contoured profile seems to be creating speed variations through increasing the central flow velocity while maintaining acceleration along the walls. This shape promotes a more controlled expansion of the gases near the walls, reducing losses and maintaining a slightly higher pressure at the wall compared to the axis.

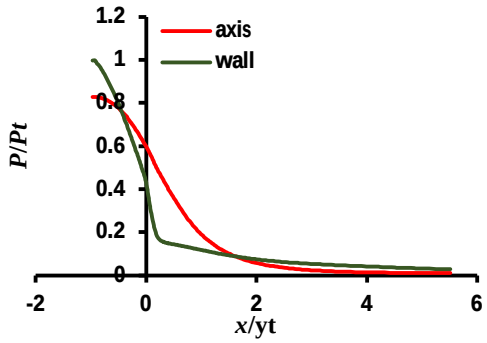

Figure 4.7 Contour nozzle: Pressure distributions along centerline and wall

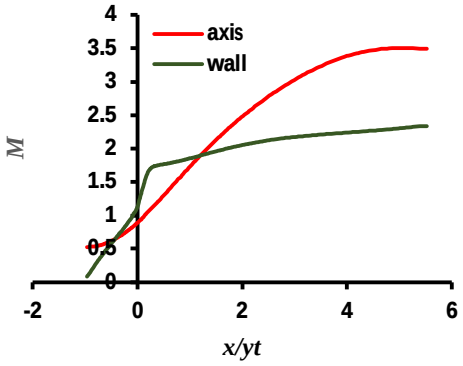

Figure 4.8 Contour nozzle: Mach distributions along centerline and wall

4.3.2 Pressure and Mach contours

The 20°- attachment angle creates a faster expansion at the beginning of the nozzle, followed by a smoother one mainly due to the 5°- exit angle. The curvature and angles create greater pressure variations than that in the case of the conical configuration (Figure 4.9). In the case of the Mach contour (Figure 4.10), it increases more significantly compared to the conical nozzle, due to the larger attachment angle. The curvature of the nozzle allows for more efficient flow expansion. The color transition in the contour indicates rapid acceleration near the inlet and gradual stabilization towards the outlet. The contoured nozzle, with its 20°-attachment angle and 5°- exit angle, is effective for quickly achieving supersonic speeds while controlling the velocity distribution to minimize losses.

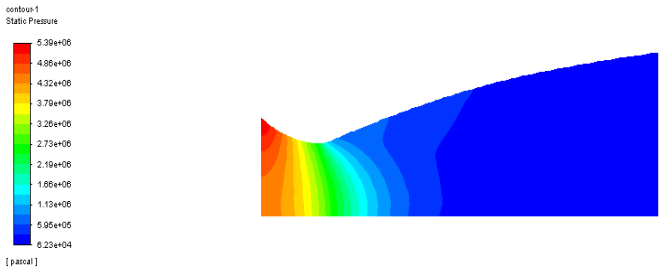

Figure 4.9 Contour nozzle: Pressure contour

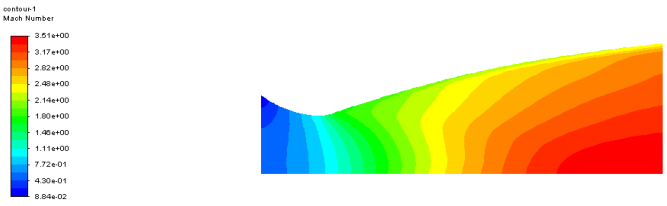

Figure 4.10 Contour nozzle: Mach contour

4.3.3 Velocity contour distributions

Figure 4.11 depicts the velocity distribution along the entire length of the nozzle, indicating a gradual increase in velocity from the inlet to the outlet. Figure 4.12 shows velocity vectors in cross-sections along the nozzle. The velocity may be seen to be greater along and around the centerline. The contoured shape of the present configuration directs the velocity towards the axis of symmetry (centerline). They, however, deviate slightly near the walls following the exit angle and guided by the divergent shape of the walls.

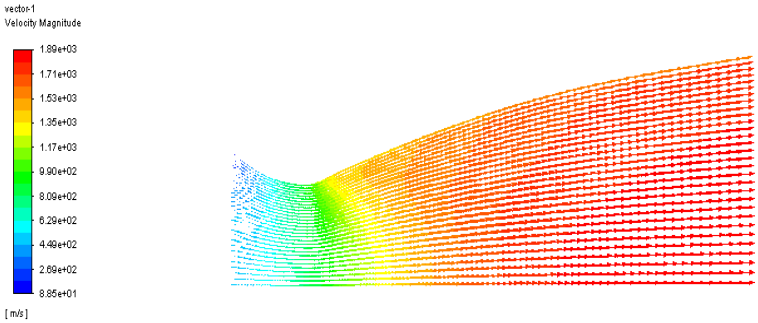

Figure 4.11: Velocity distribution along contoured nozzle

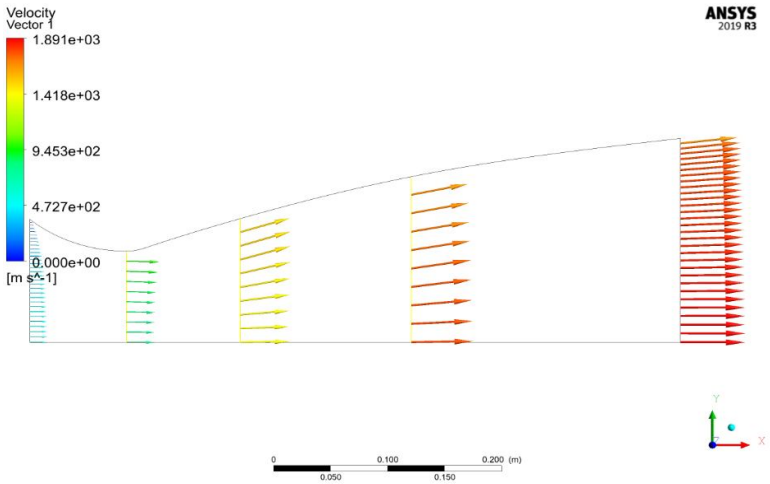

Figure 4.12: Velocity distribution along cross-sections of contoured nozzle

4.3.4 Performance parameters

Table 4.2: Contoured nozzle performance parameters

Performance parameters	Contoured nozzle
Thrust, T (N)	281,353.18
Mass flow rate, $\dot{m}$ (kg/s)	172.90
Thrust coefficient, C_T (-)	2.14
Specific impulse, I_s (s)	165.86
Effective velocity, V_{eff} (m/s)	1627.18
M_{exit}	2.33

The performance parameters of the contour nozzle are, as in the case of the conical profile, determined using the relationships derived in Section 1.6.3. They are presented in Table 4.2. The results obtained will be later compared to those gathered for the two other configurations i.e. contour and open.

4.4 THE OPEN PROFILE C-D NOZZLE

4.4.1 Pressure and Mach profiles

The curve representing the pressure distribution (Figure 4.13) shows a rapid decrease more than that of the conical and contour configurations. This configuration seems to promote faster and less controlled expansion of the gases especially near the walls (Figure 4.14). The Mach number increases very rapidly from its initial null position at the entrance. It reaches approximately 3.17 at the end of the centerline expansion and approximately 2.78 at the exit near the wall. The open nozzle, with its 15-degree attachment angle, allows for rapid gas expansion. This nozzle is shorter, and allows for a rapid increase in Mach number. It, however, leads to great energy thrust dissipation due to divergence.

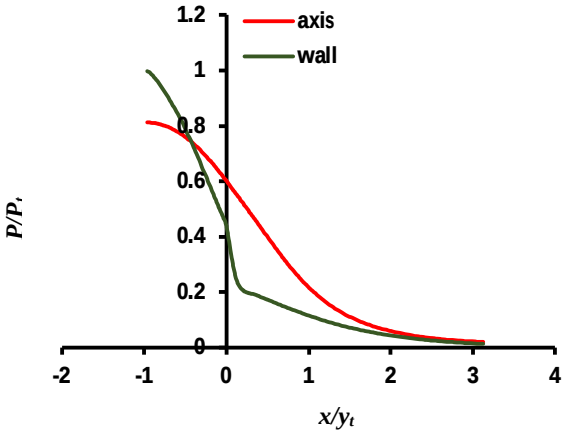

Figure 4.13 Open nozzle: Pressure distributions along centerline and wall

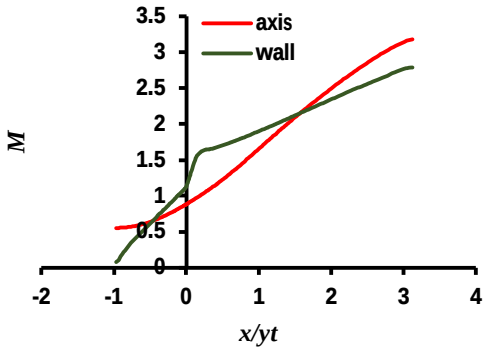

Figure 4.14 Open nozzle: Mach distributions along centerline and wall

4.4.2 Pressure and Mach contours

In this case represented by the open configuration, the pressure decreases quickly and is accompanied by an abrupt transition. The 15° attachment angle and particularly the exponential profile allows for quite a rapid expansion of gases that leads to a rapid drop in pressure (Figure 4.15). The short length of the nozzle promotes rapid diffusion, but can lead to a loss of efficiency. A fast transition from subsonic to supersonic speeds is noticed (Figure 4.16).

The open nozzle is most effective in achieving flow expansion and hence rapid acceleration, inducing higher pressure gradients. The open nozzle is the shortest of the three, which results in high flow acceleration. It can consequently be used for applications requiring rapid expansion, but it does require adjustments in order to minimize thrust loss due to divergence at the exit.

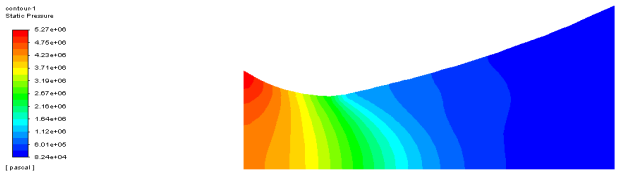

Figure 4.15 Open nozzle: Pressure contour

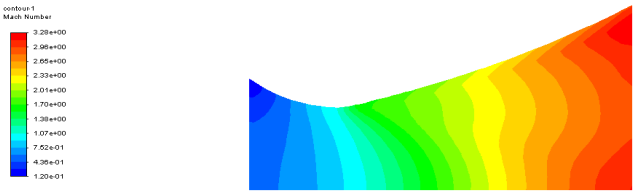

Figure 4.16 Open nozzle: Mach contour

4.4.3 Velocity contour distributions

Figure 4.17 illustrates the velocity distribution along the entire length of the nozzle, with a gradual and smooth increase in velocity from the inlet to the exit. Figure 4.18 shows velocity vectors on cross-sections at different positions. Il may be noticed the divergence of the flow field at the exit that would lead to loss of thrust due to divergence.

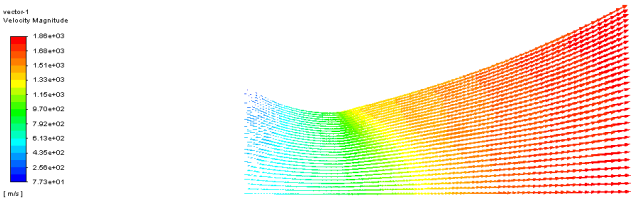

Figure 4.17: Velocity distribution along open nozzle

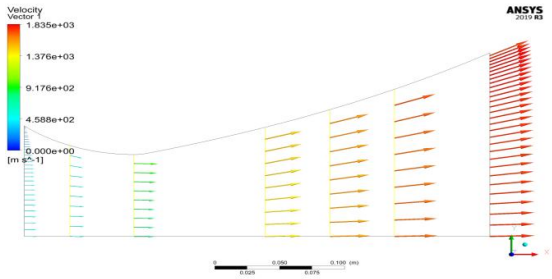

Figure 4.18: Velocity distribution along cross-sections of open nozzle

4.4.4 Performance parameters

The performance parameters of the open nozzle are, as in the case of the conical and contour profiles, determined using the relationships derived in Section 1.6.3. They are presented in Table 4.3. The results obtained will be later compared to those gathered for the two other configurations i.e. contour and open.

Table 4.3: Open nozzle performance parameters

Performance parameters	Open nozzle
Thrust, T (N)	187,715.66
Mass flow rate, $\dot{m}$ (kg/s)	96.09
Thrust coefficient, C_T (-)	1.43
Specific impulse, I_s (s)	199.14
Effective velocity, V_{eff} (m/s)	1953.60
M_{exit}	2.78

4.5 COMPARATIVE DISCUSSION BETWEEN THE THREE PROFILES

The conical nozzle provides stability and gradual expansion, making it an optimal choice for missions where a smooth transition is required. Its length allows uniform pressure management, reducing the effects of friction and gas deflection. On the other hand, the contoured nozzle with its more complex profile and its attachment and exit angles allows faster acceleration immediately downstream of the throat and controlled expansion of the gases. It therefore minimizes losses especially those due to divergence as its exit angle is the smallest (θ_e=5). This makes it an ideal choice for applications requiring high thrust.

The open nozzle, the shortest of the three, promotes a rapid acceleration represented by a fast increase in Mach number and therefore a rapid drop in pressure. This unfortunately leads to a less controlled transition. Although it offers a rapid acceleration, it can suffer from efficiency losses. It therefore may be suitable for applications-missions requiring rapid adjustments and short maneuvers.

Table 4.4: Comparison in terms of nozzle performance parameters

Performance parameters	Conical nozzle	Contoured nozzle	Open nozzle
Thrust, T (N)	279,203.67	281,353.18	187,715.66
Mass flow rate, $\dot{m}$ (kg/s)	170.78	172.90	96.09
Thrust coefficient, C_T (-)	2.12	2.14	1.43
Specific impulse, I_s (s)	166.65	165.86	199.14
Effective velocity, V_{eff} (m/s)	1634.80	1627.18	1953.60
M_{exit}	2.34	2.33	2.78

In terms of thrust coefficient that represents the control of the supersonic expansion, the open nozzle performs poorly while its contoured counterpart shows the best control (C_T=2.14). In terms of effective velocities, the open nozzle shows the highest value of this parameter. However, this performance parameter influence is lost because of the divergence at the exit that is quite large (Figures 4.17 and 4.18) that influences the thrust in the axis direction. The same conclusion may be drawn when considering the Mach at the exit section.

Taking into account all these parameters, the contoured nozzle profile stands out as the best choice. With a medium length and hence an interesting weight, it seems to be offering an

interesting compromise between the other two profiles, allowing rapid acceleration and controlled gas expansion. Moreover, it develops the highest thrust

4.5 CONCLUSION

The comparative analysis of the three configurations reveals that the contoured nozzle, with its intermediate length and high thrust, is the optimal choice. It combines a fast acceleration and a nice controlled gas expansion with a minimization of the losses due to divergence. This combination of performances makes it the most suitable profile for rocket engines and space vehicles, maximizing efficiency and overall performance.

CONCLUSIONS AND RECOMMANDATIONS

CONCLUSIONS:

The advancements observed in propulsion technology over recent years are closely tied to the efforts and developments made in both the design of contours or profiles and the analysis of aero-thermodynamic phenomena occurring within a propulsion nozzle, particularly its supersonic section. Achieving higher exit Mach numbers and significant thrusts in the shortest and lightest configurations is dependent on optimizing the performance of all engine components, especially the nozzle, which is crucial for propulsion thrust. This research primarily aims to expand the concept of simulating supersonic nozzle contours using typical equations that illustrate their contour profiles. This is achieved by defining the nozzle contours as a straight line for the conical configuration, a second-degree polynomial for the contoured configuration, and an exponential function for the open configuration. The subsonic and transonic flow fields are determined using methods based on Rao's experimental and perturbation-series development theories, respectively, while the supersonic flow is developed using the method of characteristics.

CFD simulations is performed to analyses the flow within all the configurations. The 'Ansys-Fluent' platform is applied using the Reynolds-Averaged Navier-Stokes (RANS) equations, a set of equations used in fluid dynamics to describe the behavior of turbulent flows along with a closure that applied the k-ω sst turbulence model.

The comparative analysis led to conclude that the contoured configuration is the best choice. Its relatively short length and high thrust are most effective in maximizing the performance of such configuration's propulsion nozzles. This profile offers an ideal compromise between fast acceleration, controlled gas expansion, and minimization of thrust losses du divergence.

RECOMMENDATIONS:

- Exploration of Robust and Lightweight Materials: Investigate the use of new materials that combine robustness and lightness to reduce nozzles' weight.
- **Software Development:** Improve software tools used for nozzle design and analysis, integrating more advanced features and more intuitive user interfaces.
- **New Nozzle Conceptualization:** Design new nozzles capable of controlling flow, maximizing thrust and directing it efficiently. The integration of adaptive mechanisms and smart materials could enable real-time adjustments to nozzle characteristics, thereby optimizing performance based on flight conditions.

REFERENCES

[1] T McLeod, Edward B. Introduction to fluid dynamics. Courier Dover Publications, 2016.

[2] Pontes, José, Norberto Mangiavacchi, and Gustavo R. Anjos. *An Introduction to Compressible Flows with Applications: Quasi-One-Dimensional Approximation and General Formulation for Subsonic, Transonic and Supersonic Flows*. Springer Nature, 2019.

[3] Breit, Dominic, Eduard Feireisl, and Martina Hofmanová. *Stochastically forced compressible fluid flows*. Vol. 3. Walter de Gruyter GmbH & Co KG, 2018.

[4] Genick Bar–Meir, Ph D. "Fundamentals of Compressible Fluid Mechanics." (2006).

[5] Newton, Isaac. *Philosophiae naturalis principia mathematica*. Vol. 1. ex prelo academico, typis A. et JM Duncan, 1822.

[6] Koyré, Alexandre. *Newtonian studies*. Harvard University Press, 1965.

[7] Zhang, Jiayan, Runhua Cai, and Lidan Shi. "Hybrid RANS/LES/DNS of turbulence flow along a flat plate." *Journal of Physics: Conference Series*. Vol. 2248. No. 1. IOP Publishing, 2022.

[8] phil.trans.R.Soc, Reynolds, O., (1895), 'On the dynamical theory of incompressible viscous fluids and determination of the criterion, london.A186,PP.123-164.

[9] Reynolds, Osborne. "IV. On the dynamical theory of incompressible viscous fluids and the determination of the criterion." *Philosophical transactions of the royal society of london.(a.)* 186 (1895): 123-164.

[10] ANSYS inc., Ansys Fluent Theory Guide, Release 2022R1, January 2022.

[11] Scarlatella, G., M. Tajmar, and C. Bach. "Advanced nozzle concepts in retro-propulsion applications for reusable launch vehicle recovery: a case study." *72nd International Astronautical Congress (IAC)*. 2021.

[12] On line: https://www.grc.nasa.gov/www

[13] Elger, Donald F., et al. *Engineering fluid mechanics*. John Wiley & Sons, Incorporated, 2022.

[14] Kumar, Bhupendra, et al. "Design and Computational Flow Analysis of Different Rocket Nozzle Profile." *ACS Journal for Science and Engineering* 2.2 (2022): 49-60.

[15] Anderson, John D. *Modern Compressible Flow With Historical Perspective 3rd Ed*. McGraw Hill, 2003.

[16] Elshebani, Mohammed K., and Elhadi I. Dekam. "A MOC-Based Software; Design and Evaluation of Converging Diverging Nozzles." *Journal of Engineering Research* (2020): 21-44.

[17] Haddad, A. Aérodynamique interne des prises d'air et tuyères supersoniques. I. d'Aéronautique et des Etudes Spatiales 5IAES), U. Saad Dahlab, Blida-1, Algeria, 2000.

[18] Uyeki, Devyn Yoshio Kapukawai. "A design method for a supersonic axisymmetric nozzle for use in wind tunnel facilities." *MSc in Aerospace Engg, Dept of Aerospace Engg, Dan José University* 201 (2018).